Terrestrial cosmic ray intensities

by J. F. Ziegler

Cosmic rays may cause soft fails in electronic logic or memory. The *IBM Journal of Research and Development*, Volume 40, No. 1, discussed this complex event in detail. In order to predict electronic fail rates from cosmic particles, it is necessary to know the local cosmic ray flux. This paper reviews the penetration of cosmic rays through the earth's atmosphere, and the parameters which affect the terrestrial flux. The final particle flux is shown to vary mainly with the site's geomagnetic coordinates and its altitude. The paper describes in detail the quantitative cosmic flux at one datum (New York City) and then tabulates in an appendix the relative level at other major cities of the world.

Introduction

Cosmic rays were first discovered because of the dogged curiosity of one man to explain a minor scientific irritation. The study of radioactive materials in the period from 1898 to 1912 was of widespread interest because this field offered direct insight into the nature of the atom, whose structure was still unknown. Electrometers were often used to measure the very small flux of particles coming from radioactive materials. (An electrometer consists of two thin ribbons of metal suspended in a vacuum bulb, which diverge when charge is present.) In use, electrometer readings had to be corrected for "leakage," which was dependent on the electrometer size and proportional to time, but remarkably was not dependent on the amount of charge on the electrometer foils. This leakage led to speculation about possible undiscovered radioactive contamination, or a flux of new invisible ether particles. Victor Hess studied this phenomenon by taking electrometers onto lakes where there should have been less contamination (no change in leakage) and into caves (leakage disappeared). Finally, in 1912, he brilliantly solved the problem by lifting two ion chambers in balloons to altitudes of 6 km (**Figure 1**) [1, 2]. He showed that there was indeed a flux of particles, and that it came from the sky with an intensity which increased with altitude (he was awarded the 1936 Nobel Prize for this work). His work was immediately followed by more detailed studies such as that of Kolhörster, who showed that the particle flux increased very rapidly with altitude, with a 10× increase at only 10 km. Cosmic rays became the source of wild speculation for the next twenty years because of their exponential increase in flux with height. Finally, Pfotzer showed in 1936 that the flux did not continue to increase but reached a peak at about 15 km, after which it diminished rapidly [3] [Figure 1(c)]. All of this early work is directly related to the prediction of integrated circuit (IC) soft fails at terrestrial altitudes and at airplane altitudes.

Because of the wide speculation about the nature of *cosmic rays* (a name introduced by the popular press about 1914), there is no single scientific definition of the phrase, only the popular description: *Things which rain down from the heaven and are not wet*. The scientific literature has adopted three variations on the phrase: *primary cosmic rays*, the initial particle flux external to the earth's atmosphere; *cascade cosmic rays*, the intermediate flux within the atmosphere; and *sea-level cosmic rays*, the final terrestrial flux of particles.

0018-8646/98/$5.00 © 1998 IBM

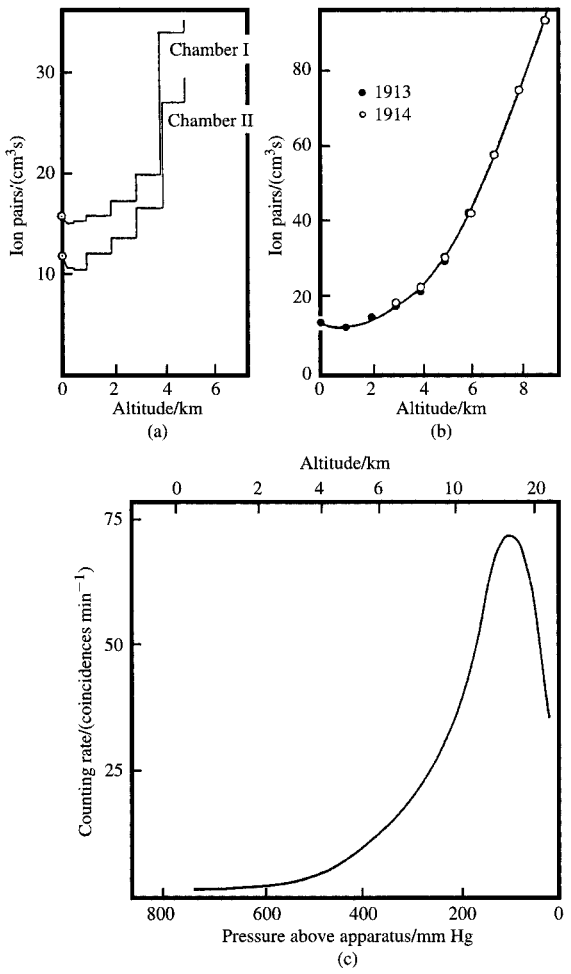

Earliest measurements of terrestrial cosmic rays. The measurement of the density of cosmic rays in the atmosphere won the Nobel Prize for Hess. In 1912 he used a balloon to take two ionization chambers up into the atmosphere to a height of 5 km, and showed that the flux of particles increased with altitude [see curves (a) and (b)] [2]. Although there were hundreds of measurements after this, it was not until 1936 that a detector was carried high enough to show that the cosmic ray flux peaked and then decreased at very high altitudes. The "Pfotzer curve" [curve (c)] was named after the scientist who showed that there was an exponential increase in cosmic rays with altitude up to about 15 km, above which the cosmic rays decreased [3]. The increase was a stunning 1000×, and for the first time it was realized how essential the thick atmosphere was to sustain stable life forms at sea level. From [2] and [3], reprinted with permission.

Outline of methodology

This paper evaluates the terrestrial cosmic ray flux at various cities to facilitate the prediction of cosmic-ray-induced electronic soft fails [4]. The cosmic particles which cause soft fails fall into the class of particles called *hadrons*, which interact with the strong interaction (also called the nuclear force), specifically neutrons, protons, and pions. Experimental values of the flux of all of these particles have never been measured for any single terrestrial site. Therefore, scattered measurements taken over 50 years must be combined with theoretical estimates of variability to obtain a single benchmark cosmic sea-level flux, the *cosmic flux datum*, which was arbitrarily chosen to be that at New York City. Other experiments and theoretical calculations will scale this datum flux to other terrestrial cities. The topics of this paper are presented in the following order:

1. *External particle flux* A discussion of the external incident cosmic ray particle flux into the earth's outer atmosphere, and how it changes with time.
2. *Cascades in the atmosphere* None of these external incident particles survive to reach the earth's surface because of the density of the atmosphere and the strength of the strong interaction. Each incident particle creates a cascade of secondary particles, which in turn creates further cascades. The details of the cascades are complicated because many high-energy particles decay spontaneously, with half-lives of less than a nanosecond. A cascade calculation is used which gives flux spectra for all significant particles (including all hadrons) in the lower atmosphere. This calculation generates the shapes of the sea-level particle flux spectra (differential flux versus particle energy). These shapes are then normalized using the available experimental data.
3. *Altitude corrections* The results of the above particle cascade calculations are used to obtain snapshots of the cascades at various altitudes in order to establish scaling rules which correct experimental flux measurements taken at various terrestrial altitudes to a common sea-level datum.
4. *Geomagnetic corrections* The earth's magnetic field deflects cosmic rays and significantly modifies the terrestrial flux. Calculations of these terrestrial variations are used to normalize cosmic flux measurements taken at various geographic locations to equivalent fluxes at New York City.
5. *NYC sea-level flux datum* The above steps establish the New York City sea-level flux datum, with experimental measurements taken at different locations and at different altitudes being normalized to a common point. No correction for solar cycle is made because the scatter of data is much larger than the effects of the solar cycle.
6. *Flux intensities for cities* The cosmic ray flux at many other cities is evaluated on the basis of their latitude, longitude, and altitude. An appendix tabulates the

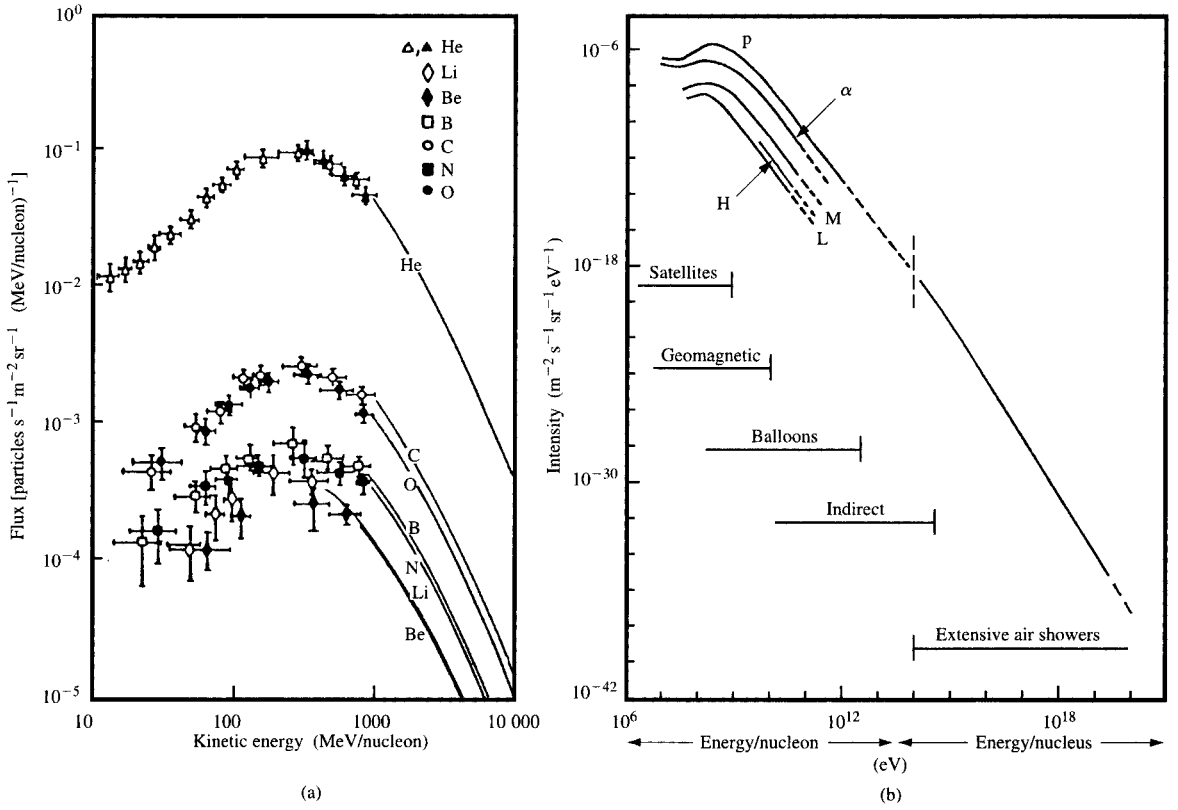

Flux of cosmic rays in space. The primary flux of particles incident on the outer atmosphere of the earth during a quiet sun period. In addition to the proton flux, there are heavier nuclei in the primary flux as shown. Figure 2(a) shows the lower-energy flux, with ions from He to O individually shown; Figure 2(b) shows much higher energies; proton flux = p; He flux = α; light ions ($Z = 3-5$) = L; medium ions ($Z = 6-9$) = M; and heavy ions ($Z > 9$) = H. Summed together, the heavier nuclei add enough neutrons to the primary proton flux to make the primary flux average 70% protons and 30% neutrons. From [5] and [6], reprinted with permission.

results for many cities with populations above 500 000 or isolated sites with extensive electronic systems (e.g., Kinshasa, Zaire, or Leadville, Colorado).

Primary cosmic ray flux

There are two sources of primary cosmic ray particles: First, there is a flux of very energetic particles from distant sources in the galaxy. There is also the flood of low-energy particles called the *solar wind*, which disappears during the period of the quiet sun, and then builds into a torrential storm of particles during an active sun period. These two particle currents are initially considered separately.

- *Galactic flux*

The galactic cosmic rays are of debatable origin, and there are no theoretical estimates of the primary flux. Some have energies beyond 10^{23} eV, so exotic scenarios have been proposed for their origin, such as being accelerated by stellar flares, supernova explosions, pulsar spin-offs, or from the explosions of nascent galactic nuclei. The flux density of primary cosmic rays in the galaxy is very large, about 100 000/m^2-s. The *energy density* of cosmic rays is very high, more than 1 MeV/m^3, so it is assumed that they must originate within our galaxy or else the mass/energy balance of cosmology would be inconsistent with current theory. Because our galaxy is spinning, it is saturated with a magnetic field of several microGauss. The cosmic rays interact with this field so that, typically, they continuously spiral during their lifetime with a spiral diameter of a fraction of the galactic diameter. It is because of this vast spiraling trajectory that a local observer within the galaxy would detect that the galactic cosmic rays are isotropic and do not come from particular sources.

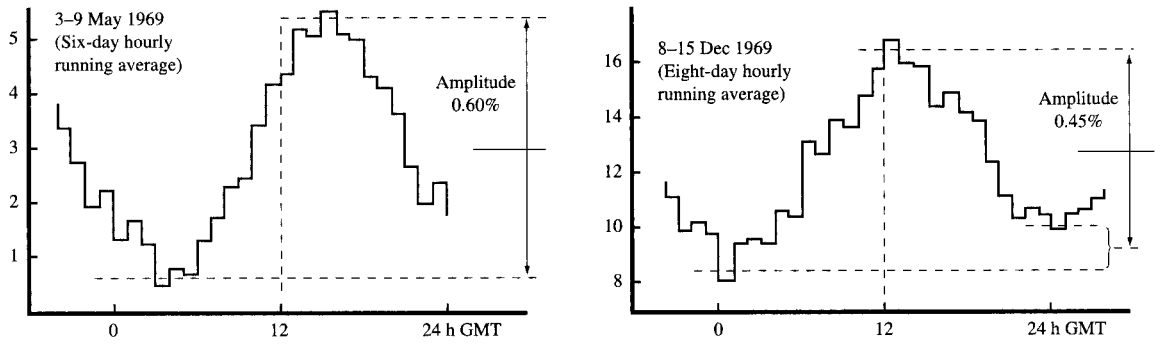

Figure 3

The sea-level flux of hadrons is measured for the earth near apogee and near perigee during an active sun period. These data have been averaged hourly for about a week in each case, averaging 1×10^6 counts per hour. The plots show the measured count rates, greatly expanded to show the average daily variations (the ordinate scales are arbitrary). Both sets of data show a peak at about noon and a minimum at midnight, which clearly is due to the solar wind of particles. But the amplitude is less than 1%, indicating that the sun is a minor source of sea-level hadrons. Note that the minima do not have the same absolute levels because of a drift with time of the total cosmic ray flux. Extracting such small variations from the much larger total flux often leads to asymmetries. From [18], reproduced with permission.

Table 1 Recent periods of the solar cycle.

Active sun	*Quiet sun*
1958	1963
1969	1974
1980	1985
1991	1996

Particle detectors in satellites have determined that the primary low-energy cosmic ray particles consist of 92% protons and 6% alpha particles, with the remainder being heavy nuclei (**Figure 2**). There are no free neutrons in the external galactic flux because neutrons are unstable unless bound in a nucleus and have an 11-minute half life as free particles. The flux of higher-energy particles shown in Figure 2 has been estimated from various kinds of experiments: (a) the flux variation of particles through different strengths of the earth's geomagnetic field; (b) data from large-particle spectrometers flown in balloons to altitudes of 100 km; (c) measurements of the penetration of hadron cascades into the earth (marked *Indirect* in Figure 2); and (d) the analysis of the very large individual showers with 10^8 particles which spread over a hundred kilometers at sea level (all from a single incident particle!). Accurate spectrometers in satellites such as CREDE-II have identified the individual elements in the primary flux, and typical data are shown in Figure 2(b).

These incident particles have such high energies that the particles have deBroglie wavelengths smaller than a proton diameter (or, more explicitly, smaller than the interaction distance of the strong interaction). Further, their energy is far greater than that of nuclear binding energies. This means that when a cosmic ray alpha particle hits an atmospheric nucleus, the alpha particle need not be considered as a He nucleus, but can be treated as independent particles, two protons and two neutrons, with each one interacting independently with any atmospheric nucleus. Therefore, from the standpoint of its interaction with the atmosphere, we can simplify the primary particle flux distributions of Figure 2 by assuming that the incident flux is just 71% protons and 29% neutrons. This assumption, along with corrected energy/flux curves for just two sets of particles, greatly simplifies the calculation of the atmospheric cascades. Calculations of cosmic ray particle trajectories in the earth's magnetic field indicate that initial energies above 1 GeV are necessary for penetration to the earth's surface (see [7–16]). Precise satellite measurements show that the incident flux of cosmic rays with energies above 1 GeV is about $1600/m^2$-s at the edge of the exosphere with isotropic trajectories [17].

- *Solar flux*

A second source of primary cosmic rays is the sun. During the quiet sun period there are essentially no energetic particles in the solar wind which can reach sea level on earth because of the low energies of the particles. In the active sun period, the solar wind increases by factors of the order of 10^6, making it far denser than the galactic particle flux. The sun has a variable cycle which ranges

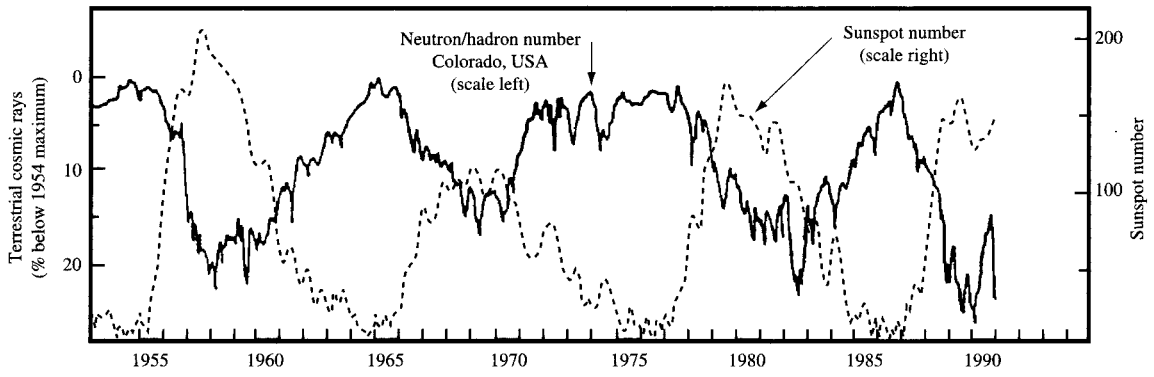

Figure 4

Shown are 35 years of solar sunspot activity, which defines the solar cycle, and the terrestrial flux of hadrons (mostly neutrons) in Colorado, USA. The two data envelopes are counter-cyclic. The solar cycle has been unusually short in the last 30 years, which may be the main factor in global warming (much to the chagrin of the environmentalists). Note that the terrestrial flux of hadrons has ordinate units of "% below 1954... minimum" and shows a maximum effect of the solar cycle on the particle flux of about 25%. Decreases to 30% were seen from June through December 1991 during the period of the greatest solar activity ever recorded. (Data from J. Simpson, University of Chicago, unpublished.)

from 9 to 12 years; **Table 1** shows the years of the most recent cycle nodes. During the previous quiet sun period, 1985–1986, satellite detectors indicated that there were effectively no energetic particles in the solar wind which could penetrate to sea level on earth (i.e., with energies greater than 1 GeV).

The simplest evidence that solar particles do not induce sea-level cascades is that there is only a small diurnal change. The maximum diurnal effect is estimated at less than 1%; see **Figure 3**, which indeed shows minima occurring every day at local midnight. During periods of a large solar flare (which might last a few days), there is a small chance that the earth might pass through the narrow beam of particles from the flare, and the total intensity of cosmic rays at the earth's surface might double for a few hours. More than two dozen of these events occurred during 1990–1991.

However, there is a more important aspect to the solar cycle than the increased particle flux. The active sun with its large solar wind creates a large distortion of the magnetic field about the earth (the magnetosphere), which increases the earth's shielding against intragalactic cosmic rays. This leads to a net *reduction* of the sea-level cosmic rays during the period of the active sun. In the active sun of 1989–1991, which was the most intense solar activity ever recorded, the sea-level intensity of cosmic rays actually *decreased* by about 30%. Thus, the active sun greatly intensifies the solar wind, and the external particle flux increases, but the earth's distant magnetic field also increases. The final result of this complex interaction is that the terrestrial sea-level flux of cosmic particles *decreases during the active sun*, except for the few hours during the most spectacular solar flares (**Figure 4**).

Figure 4 is also a good representation of how the terrestrial flux which causes soft fails changes with the solar cycle. It includes all hadrons, and also has a significant contribution from muon capture processes (described later). It shows that the solar cycle is a perturbation of the general terrestrial flux, amounting to, at most, a 30% reduction during the most active solar periods. The data in Figure 4 constitute the longest continuous record of cosmic rays [19–21]. The figure shows the general inverse correlation between solar activity and terrestrial cosmic rays, but the details of the two phenomena have only partial relationships. This is because the sunspots, and their corresponding solar flares, usually distort the solar magnetosphere only in specific directions, and the effect on the earth depends on whether the earth is in that sector.

Solar flares may also send a particularly intense stream of particles into the solar wind, but these particle streams are usually of such low energy that they are not detected at sea level. During the period from 1956 to 1972 (17 years) there were 61 solar events which caused particle bursts at satellite altitudes. Of these, only 18 were simultaneously detected at sea-level particle detector stations, with an average change of flux of about 10% for a period of about a day ([17], p. 6-20/21). More typical is

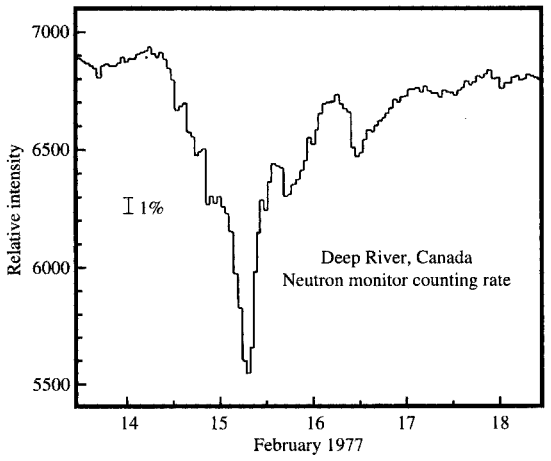

Figure 5

Illustration of a sea-level cosmic ray Forbush decrease. Forbush analyzed sea-level cosmic ray intensities over the period from 1937 to 1952 and found correlation between narrow flux dips, such as shown above, and particular types of solar events. He hypothesized that the dips were due to temporary increases in the magnetosphere strength due to the solar events [22].

Table 2 Active particles in a cosmic ray cascade.

Particle	*Interaction type*			*Mass* (MeV)	*Lifetime*
	Electromagnetic	*Strong*	*Weak*		
Pions	•	•		≈134	≈26 ns
Muons	•		•	≈106	≈2 μs
Neutrons		•		940	12 min
Protons	•	•		938	stable
Electrons	•			0.5	stable
Photons	•				stable

a *decrease* in particle flux due to increased intensity of the magnetosphere caused by the solar event. Typical sea-level particle flux changes are shown in **Figure 5**, in which a narrow 20% dip is due to a solar flare event. This type of decrease is called a *Forbush decrease*, after the scientist who first related the decrease to solar flares [22].

Details of the variation of the primary galactic particle flux with the solar cycle have been measured, and above 1 GeV there are almost no significant differences due to the solar cycle.

Cosmic ray cascades in the atmosphere

The earth's atmosphere consists of about 1033 g/cm^2 of oxygen and nitrogen, with a density that changes with altitude. In cosmic ray physics, altitude is usually considered in units of g/cm^2 of the atmosphere above a given height. Sea level has an altitude of 1033 g/cm^2, and Denver has an altitude of 852 g/cm^2. (For reference, 1033 g/cm^2 = 1013 mbar = 29.92 in. Hg = 760 mm Hg.)

The incident particles, protons and neutrons, interact with atmospheric matter primarily with the strong interaction, which has an interaction length of about 1.2×10^{-13} cm. The particles which are considered active in a cosmic ray cascade are reviewed in **Table 2**.

One simple cascade model is to consider the earth's atmosphere as condensed nuclear fluid. One removes the electrons, which are mostly irrelevant to the showers, and allows the remaining atmospheric nuclei to condense. The nucleons (protons and neutrons) are separated by the radius of the nuclear force, 1.2×10^{-13} cm. The nuclear force is so strong that if another hadron (any particle which is sensitive to the nuclear force) comes within this distance, the probability of a reaction is unity, and the result is that the old particle disappears and is replaced by one or more new particles, possibly of a different type. The atmosphere is so thick that its condensed nuclear fluid is about five layers thick. This means that, on average, each incident particle generates five successive generations of showers. However, the particle flux of hadrons does not increase this much because of fundamental conservation laws, and most of the increased cascade flux is in electromagnetic and weak interacting particles. For example, by sea level the non-hadron particles, especially muons, outnumber all the hadrons by 200×. Further, once the hadron energy drops below 100 MeV, it is lost from the cascade because it is rapidly absorbed.

Thus, each high-energy particle rapidly generates large cascades which increase in particle density until sea level is reached (**Figure 6**). However, the hadron component increases slowly, until a maximum density is reached at about 15 km, and then it decreases because of low-energy hadron absorption by nuclear reactions.

At this point we summarize the steps used in calculating the generations of cascades in the atmosphere from a single incident nucleon. For those interested primarily in the final terrestrial fluxes, it is best to look at Figures 6 through 8 and skip to the next section, *Variation of terrestrial cosmic rays with altitude.*

Typically, the most important atmospheric hadron interactions for energies above 100 MeV are

$$\begin{aligned} \mathrm{p} + \mathrm{air} &\rightarrow \upsilon_{\mathrm{p}} + \upsilon_{\mathrm{n}}\mathrm{n} + \upsilon_{\pi^\pm}\pi^{\pm} + \upsilon_{\pi^0}\pi^0, \\ \mathrm{n} + \mathrm{air} &\rightarrow \upsilon_{\mathrm{p}} + \upsilon_{\mathrm{n}}\mathrm{n} + \upsilon_{\pi^\pm}\pi^{\pm} + \upsilon_{\pi^0}\pi^0, \end{aligned} \quad (1)$$

where p = proton, n = neutron, air = either O or N nucleus, υ_x = neutrino of type x, $\pi^{\pm}$ = charged pion, and π^0 = neutral pion. Thus, the incident particle is converted to several unstable particles, many of which will collide

before they spontaneously decay. Most of these decay before a subsequent interaction (a pion lifetime is about 10^{-9} s), with the following spontaneous decay reactions:

$$\pi^{\pm} \rightarrow \mu + \upsilon,$$

$$\pi^{0} \rightarrow 2\gamma \rightarrow \text{electromagnetic showers},$$

$$\upsilon_x \rightarrow e + 2\upsilon \rightarrow \text{electromagnetic showers}. \qquad (2)$$

Secondary production spectra for type-q particles are estimated by

$$G_{ql} = I_q E_B^l U(E_B - \eta_q),$$

$$G_{qj} = 2\pi \int_0^{\pi} d\theta \sin\theta \, F_{qj}(E \rightarrow E, \Omega),$$

$$\Omega = \cos\theta, \qquad (3)$$

where G_{qj} is the secondary production spectrum of type-q particles integrated over the solid angle; particle q = p, n, π, μ, e, γ; I_q is the flux of type-q particles; E is the energy of particle B at height l; $U(x)$ is the Heaviside function, with the restriction that $U(x < 0) = 0$ and $U(x > 0) = 1$; η_q is a lower-energy limit below which secondary particle production is cut off; qj = interaction type np, pn, πn, πp, $\mu\pi^{\pm}$, $e\mu$, $\gamma\pi^{0}$, $e\gamma$, γe; and θ = angle of scatter into solid angle Ω.

The above reactions dominate all of the cascades for particles above 0.1 GeV, below which energy particles are rapidly absorbed in nearby collisions and lost from the showers. Other, lesser reactions which are included in our cascade calculations can be found in more extensive cascade calculations [23–26]. These publications also estimate the cross sections for all of the inelasticities and multiplicities for hadron–air collisions.

Charged-particle energy loss in transiting the atmosphere is simplified in our calculation by assuming that the atmosphere is composed of a single nuclear species with an atomic weight of 14.48, an atomic number of 7.31, and an ionization potential of 86.8 V. Because oxygen and nitrogen are so close in the periodic table, this assumption yields a good approximation [27].

The particles which have the strong interaction lose energy very rapidly to atmospheric nuclei, and their energy is dissipated into nuclear fragments. Those which interact through the electromagnetic interaction lose energy constantly to the atmospheric electrons. The heavier particles are least deflected, causing tight dense cascades, and the light particles form a more diffuse halo about the heavier particles (**Figure 7**). All energetic cosmic rays at sea level appear in cascades or groups of particles which hit a location simultaneously, i.e., in less than a nanosecond. *At sea level, there are about eight cascades/m^2-s.*

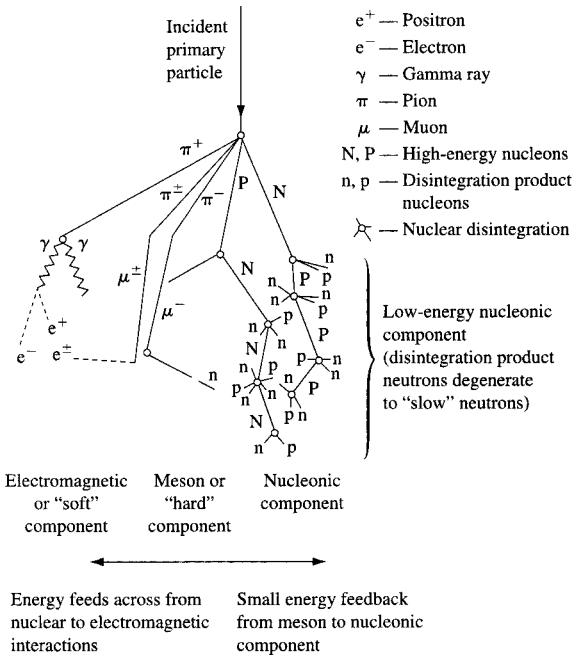

Figure 7

Schematic representation of several possible branches of the atmospheric cosmic ray cascade. On the left are several examples of secondary π^- particles which spontaneously decay in about 10^{-9} s into electromagnetic particles, or yield non-hadron particles. On the right, a π^- interacts with a nucleus to start a nucleonic cascade, and a secondary neutron interacts with a conventional hadron cascade. The notation indicates which cascades contribute mostly to the electromagnetic interactions, and which to the hadron cascade component.

The results of our calculations may be illustrated by the calculation of the spectrum of particles at New York City (**Figure 8**). This calculation shows the four most important particles and their relative abundance. Muons dominate the medium- and high-energy portions of the spectrum. There are hundreds of times more muons than any other high-energy particle. This is because the muons do not have the strong interaction and they lose energy only gradually to the atmospheric electrons. There are the same numbers of neutrons and protons at very high energies, but below 1000 MeV the absolute proton flux becomes less than the neutron flux because of the proton's additional electromagnetic interaction with the electrons of the atmosphere. The pion flux is small relative to the flux of other particles because the pion lifetime of several nanoseconds causes most of them to fragment spontaneously before reaching sea level. Finally, it should be noted that all particle fluxes below 100 MeV are very sensitive to local environments, i.e., the material of nearby

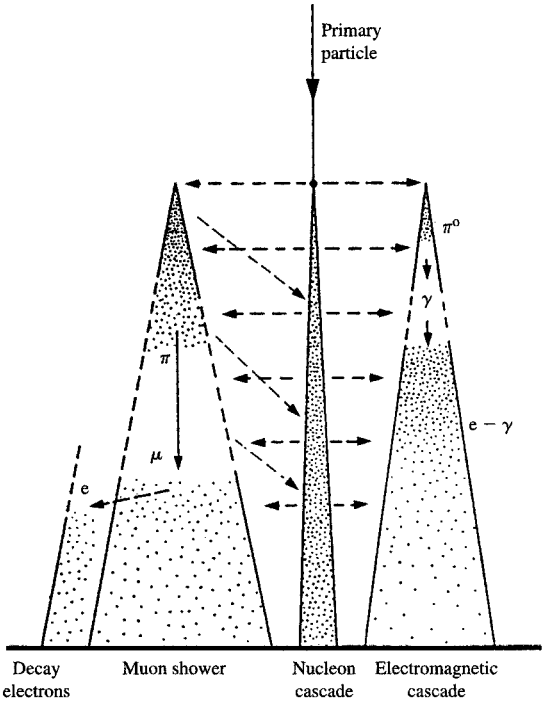

Figure 7

Schematic of cascades of various particles. The particle cascade from a very energetic primary particle can be described as a series of concentric cones. The innermost cone contains the heavy nucleonic particles of the cascade, and this is surrounded by cones which describe the relative spread of pions, then muons, and finally the light and easily scattered electrons. The figure shows these schematically, with the cones separated for clarity. Arrows also show where energy may be transferred from one cone to another as the cascade progresses. In Australia and South Africa there are cosmic ray detector arrays spanning hundreds of kilometers. These arrays measure cascade size, finding cascades as big as 100 km, which indicates an initial particle energy greater than 10^{22} eV!

walls, ceilings, and floors, so the results for these low-energy particles are probably accurate only to within an order of magnitude.

Note that in Figure 8 the latitude and longitude of New York City are shown also in the equivalent geomagnetic values. *The geomagnetic coordinates assume a sphere centered on the earth's magnetic pole rather than on its spin axis*. In 1980, the north magnetic pole was located at 78.32 N and 68.95 W [17]. (Note: Latitude and longitude are quoted in *fractional degrees* if specified as 78.32, and in *degrees and minutes* if specified as 78-32 or 78° 32′.) The magnetic field of the earth is found to cause a variation of the sea-level flux of cosmic rays by about 400%; for this correction, we must deal with geomagnetic coordinates (see below).

Table 3 Sea-level particle absorption lengths.

Particle	*Length L* (g/cm^2)
Electrons	100
Protons	110
Pions	113
Neutrons	136
Muons and muon capture	261

Also given for New York City in Figure 8 is the notation GMR, which stands for geomagnetic rigidity. This concept is discussed later in the section on latitude effects on cosmic ray fluxes.

Variation of terrestrial cosmic ray flux with altitude

It was noted that less than 1% of the primary galactic particles can create a cascade which reaches sea level. The cascades do not continue to increase in size as they penetrate the atmosphere, for there are also many absorption processes. Most of the particles either decay spontaneously (pions have a mean lifetime of nanoseconds, muons about a microsecond), or they lose energy and reach thermal energies before reaching earth, so that these particles are lost from the cascade. The maximum cascade density of particles occurs at an altitude of nine miles (15 km), or just above airplane altitudes. This is called the Pfotzer point [4] (Figure 1). Below this, there is a net loss of total hadrons in the cascades. We discuss the cascades in this lower region of the atmosphere in detail, for it determines the variation in the flux of particles at terrestrial sites. By examining the variation in flux with altitude using Boltzmann transport calculations, we find that simpler approximations may be made. In the lower atmosphere the calculations show that the cascades follow what is called *linear cascade propagation*. This means that creation and loss of particles can be treated by simple differential equations, and the changes in flux of particles may be simply expressed in a quantity called an "*attenuation factor*" or an "*absorption length*" L, which combines the creation and absorption processes into a single parameter that allows the calculation of the net change of particle flux with atmospheric pressure or altitude:

$$I_1 = I_2 \exp\left(\frac{A_2 - A_1}{L}\right), \tag{4}$$

where I_1 is the cascade flux at some altitude (pressure) A_1, and I_2 is the flux at altitude A_2, both altitudes normally

Table 4 Particle flux ratio: Denver/New York City.

Particle	*Percentage*
Electrons	+611
Protons	+518
Pions	+498
Neutrons	+378
Muons	+142

being expressed in g/cm^2. To convert terrestrial altitudes to atmospheric pressure, g/cm^2, we have derived the simple fitted equation

$$A = 1033 - (0.03648H) + (4.26 \times 10^{-7}H^2), \quad (5)$$

where A is in g/cm^2 and H is in feet (this assumes an average barometric pressure and a temperature of 0°C). For the lower altitudes, we calculate typical absorption lengths (also called attenuation lengths) using our Boltzmann transport equations; see **Table 3**.

The absorption lengths of various particles are different because of the strength of their interaction with the atmosphere, and their mass. A larger absorption length means slower attenuation, and hence less difference in flux when we compare locations with different altitudes. As an example of the magnitude of these factors, the increase in cosmic ray flux from New York City (0 feet = 1033 g/cm^2) to Denver (5280 feet = 852 g/cm^2) is shown in **Table 4**. To compare the total hadron flux at these two cities, these flux changes must be multiplied by the absolute sea-level flux for each type of particle. This will cause the hadron increase from NYC to Denver to be about a factor of 4.

The proton + pion relative portion of the cosmic ray nucleon flux increases with altitude, and the muon-capture portion decreases. At altitudes such as that of Leadville, Colorado, elevation 10 151 feet, the proton + pion portion of the nucleon flux is about 30% of the total flux, as compared to <5% at sea level.

Variation of terrestrial cosmic ray flux with geomagnetic location

The ability of charged-particle radiation to penetrate the magnetosphere from the outside is limited by the earth's magnetic field. Particles with a low magnetic rigidity (i.e., momentum per unit charge) are turned back by the field, so they are unable to penetrate to terrestrial altitudes. For each point in the magnetosphere and for each direction of particle trajectory to that point, there exists a threshold value of magnetic rigidity, called the *geomagnetic cutoff*. Below this momentum value, no charged particle can reach sea level [29].

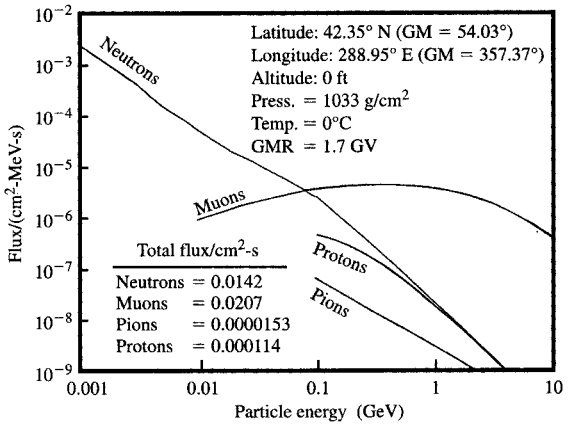

Figure 8

Theoretical sea-level cosmic rays. Theoretical calculation of the flux of cosmic ray particles at New York City. The most abundant particles are muons, which physically act like heavy electrons except that they are unstable and have a lifetime of less than 2 μs. The next most abundant particles are neutrons, which are very penetrating because they are neutral and do not lose energy to the electron sea of the atmosphere. There are just as many protons as neutrons produced in the upper-atmosphere cosmic ray showers, but the protons are charged and hence constantly lose energy to the atmospheric electrons and disappear faster than the neutrons at lower altitudes. The pions, like the muons, are unstable, and there are 100 muons for every pion at sea level, but pions are far more effective in causing soft fails in electronic circuits [28]. All flux curves below 0.1 GeV have limited accuracy because local building materials can vary the absorption and production of the particles by more than 10× [26].

The first geomagnetic cutoff was computed by Stormer in 1930 [30], and since that time this field has become a long-term endeavor for various scientists [7–16]. The U.S. government has sponsored research in this field for 50 years because of its implications for long-distance communications. The most accurate values to date are probably those of Shea and Smart, who use a three-dimensional model of the magnetosphere and massive ray-tracing algorithms to establish geomagnetic cutoffs. Their work is updated every five years to incorporate changes in the distribution of the magnetosphere. (This is discussed in detail in the section on calculation of geomagnetic rigidity.)

These calculations of geomagnetic cutoffs are always for a quiescent sun. Solar flares cause major distortion of the magnetosphere, and this has been treated in detail to show how the cutoffs should be increased depending on simple parameters of the flare [31]. The assumptions of this treatment are crude, but since the effect is, at most, a factor of 2 increase in terrestrial flux for the few days the

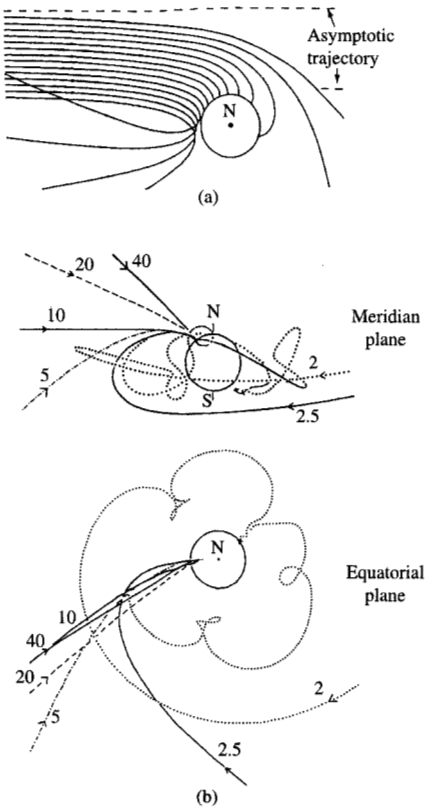

Figure 9

The trajectories of incident cosmic rays are quite complex because of the earth's magnetic field. The above diagrams illustrate the paths which would be taken by particles with the same initial charge and momentum. Part (a) illustrates the paths of parallel 20-GV protons incident along the earth's equator; part (b) illustrates the more complex calculations which are done to evaluate the minimum energy needed to penetrate to sea level. The rigidity of each proton (in GV) is indicated beside its track. (It is assumed that if the primary particle cannot make it to sea level, none of its possible cascade progeny can reach sea level either.) The geomagnetic rigidity of a site is the minimum momentum which is required so that one of the protons reaches sea level, assuming the incident particles are isotropic and considering all incident trajectories. Typical momenta are 0 GV for magnetic poles and 1 GV for the latitudes within 20 degrees of the poles, increasing to almost 20 GV at the geomagnetic equator. Particles with momenta below these rigidities cannot produce cascades which reach sea level. From [32], reproduced with permission.

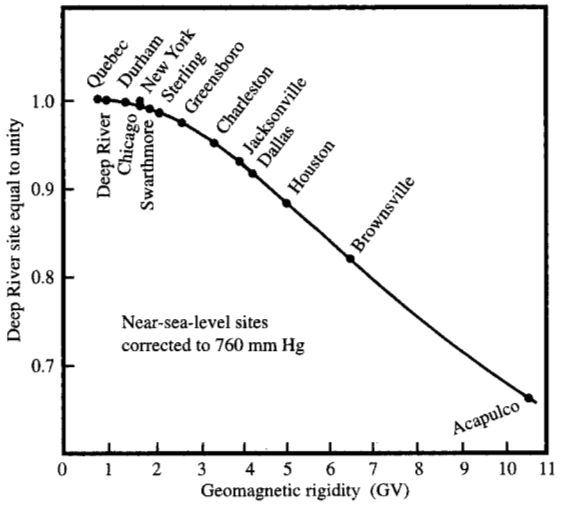

Figure 10

One of the earliest experimental evaluations of the variation of the sea-level cosmic ray hadron flux (ordinate scale) with geomagnetic rigidity (abscissa). The data were produced by hauling a 23 000-lb detector to the various locations shown. At half of these locations there was also a large cosmic ray station to verify the calibration of the mobile detector. The detector used was very sophisticated and reliable, and was designed to be sensitive only to nucleons with energies above 50 MeV. The resulting curve shows the variation of cosmic ray hadron flux with geomagnetic rigidity. From [35], [36], reproduced with permission.

flare is prominent, no one has published a more detailed assessment.

The earth's magnetic field forms a shield against charged particles everywhere except for particles vertically entering a magnetic pole. As a primary cosmic ray particle approaches the earth, the magnetosphere interacts with the particle's charge and bends the particle's trajectory as shown in **Figure 9**. If the particle hits an atmospheric atom and starts a cascade, each of these charged particles will also have its path bent. This bending increases the possibility that the particles will end up going back out into space, and also lengthens the cascade path, reducing the probability that particles will reach sea level.

The effectiveness of the earth's magnetic shield in reducing sea-level cosmic showers is discussed in terms of the primary proton's "rigidity," defined as pc, where p is the proton momentum and c is the speed of light. The customary units of rigidity are volts. Since the primary protons which can cause a sea-level shower are all highly relativistic, we can simplify this discussion by assuming their energy to be the same as their rigidity, but with the units changed from eV to V, or from GeV to GV.

GEOMAGNETIC RIGIDITY is the minimum energy a primary proton must have to create a cascade which can reach sea level at that location.

A difference in the sea-level cosmic ray flux between Anchorage and Tokyo can be understood by noting different rigidities. Primary cosmic particles with energies from 1 to 12 GV may penetrate to Anchorage but cannot penetrate to Tokyo; hence, Anchorage is exposed to more

sea-level cosmic rays. Once this is understood, it is a matter of modeling details to evaluate the exact difference. This is done by considering particles with isotropic trajectories hitting the atmosphere above each city and evaluating their cascades through the atmosphere, but with the energy cutoff of each cascade determined by the geomagnetic rigidity of that location. (This is discussed in the section on theoretical calculations.)

There have been hundreds of experiments evaluating the concept of geomagnetic rigidities (in the early days this was called "the latitude effect"); a typical example is shown in **Figure 10** [33, 34]. Many studies were undertaken under the auspices of the International Geophysical Year (IGY 1957–1958) and the International Quiet Sun Year (IQSY 1964) [37–51]. The *latitude effect* was clearly seen, and the variation with solar cycle was outlined. However, these experiments are complicated to undertake, and every time a comprehensive set of experiments was published, within a few years there was a paper showing a major flaw in the results. For example, later work indicated that the result shown in Figure 10 was erroneous, since major corrections were not applied. There should have been at least 5% variation between the various sites and the solid line, but the data shown appear to have a data-to-line fitting accuracy of better than 1%.

The measurement of the sea-level hadron flux variation with latitude is very complicated, and we jump from this first effort to one of the final comprehensive efforts shown in **Figure 11** [33, 34]. The inverse of the hadron flux attenuation length is plotted in units of percent/mm of Hg—see the ordinate values on the right side of the plot to convert to an attenuation length in units of g/cm^2. The plot shows attenuation length vs. altitude and vs. geomagnetic rigidity, with both the calculations and the many data points coming together with remarkable consistency. At sea level (right side of the plot at 760 mm Hg), the nucleonic attenuation length varies from 137 g/cm^2, for a geomagnetic rigidity of 1 GV, to 157 g/cm^2 for 13 GV. The attenuation length varies with rigidity because higher-energy primary particles create cascades with higher mean energies which have slightly lower interaction cross sections with the atmosphere and hence longer mean free paths. As pointed out before, the difference between attenuation lengths of 137 g/cm^2 and 157 g/cm^2 would make the relative flux of cosmic rays at Denver vs. New York City vary by only 10% from the mean. Therefore, this difference, due to geomagnetic considerations, is only marginally important for electronic soft-error evaluations. (Note: There is a further correction in this attenuation length estimate at sea level which is discussed below.)

Also shown in Figure 11 is the effect of altitude on the mean free path of nucleons. As altitude increases (lower pressure on the abscissa), the attenuation lengths increase up to an altitude of 11 000 ft (500 mm Hg). This increase has been attributed to the fact that the high-energy proton/neutron ratio in the cascades increases with altitude (at sea level the high-energy neutron/proton ratio is 5×, while at Denver it is about 3×), and the protons have a much lower mean free path than the neutrons because of their electronic energy loss. This lowers the total nucleon attenuation length.

Above 11 000 ft there is a decrease of the attenuation length because the mean energy of the cascades is increasing with altitude and this increases the mean free path of the cascade nucleons. Cascades with higher energy are more penetrating. The increased penetration of higher-energy cascades is also seen in Figure 11 in the change of attenuation length with geomagnetic rigidity. At sea level, the value of L for neutrons is about 137 g/cm^2 for GV = 2, and about 156 g/cm^2 for GV = 13. The cascades at a 13-GV location have a higher mean energy at sea level than those at a 2-GV location, and the higher mean cascade energy means a higher attenuation length, i.e., less attenuation [33].

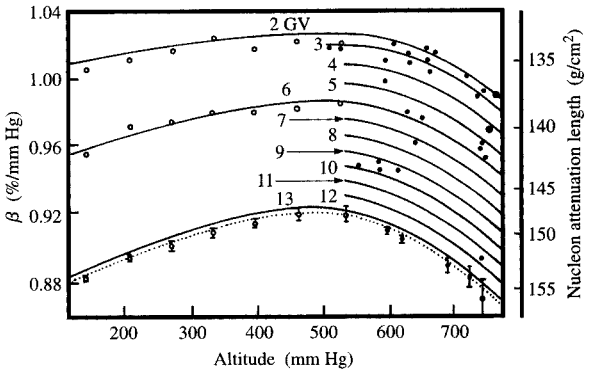

Figure 10

Cosmic ray intensity vs. altitude and rigidity. This figure is from the most comprehensive study ever made of the attenuation of cosmic rays on earth [33]. Data from most of the locations described in Figure 10 were combined with data from other mobile nucleon detectors on ships and airplanes to map out most of the earth. The detectors were believed to be sensitive only to hadrons with energies above 50 MeV. The data were then fitted, allowing only two free parameters: one for latitude and one for altitude. This analysis produced the solid lines, which show the nucleon attenuation coefficient β as a function of altitude and geomagnetic rigidity. This is because both affect the energy distribution of the cascades, and the details of attenuation are energy-dependent. This beautiful study is like the last apple of the season: It is rich with flavor and detail, but it also contains a worm (see Figure 12). From [33], reproduced with permission.

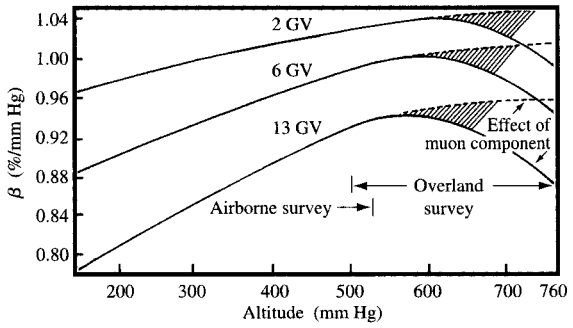

Figure 12

Mean attenuation coefficient for neutrons. An analysis of the results presented in Figure 11 showed that the proposed attenuation curves (solid lines in Figure 11) could indeed accurately predict the differences in nucleon flux recorded by the IGY detectors. However, the detectors did not accurately discriminate against other particles which were not nucleons. The most important example was an event called muon capture (see text), which generated neutrons within the detector. This figure shows how the attenuation coefficients must be altered so that they can be used to correctly predict the change of nucleon flux with altitude and geomagnetic rigidity. The muon capture effect disappears with altitude because its magnitude remains fairly constant with altitude, while the neutron flux continues to increase, finally making the muon capture error negligible. With this correction, the mean attenuation lengths should be accurate to about 1% [33, 52, 53]. From [33], reproduced with permission.

Experiments similar to that described above have been done aboard a ship sailing in the South Atlantic and Indian Oceans,[1] measuring the nucleon attenuation coefficient in the Southern Hemisphere as a function of rigidity. The results are virtually identical to those of Figure 11, which creates confidence that the experiments were producing reliable values.

A final matter makes the all-purpose attenuation lengths of Figure 11 a little less attractive than they seem. These attenuation lengths describe the IGY/IQSY nucleon detector response with high accuracy, but they do not remove instrumental error, which was just being discovered when IGY/IQSY was ending. One major error was the generation of neutrons by muon capture within the detector. This reaction is one in which a negative muon combines with a proton and produces one or more neutrons inside the detector. About 7% of the measured sea-level neutrons were from this cause.

The corrections to Figure 11 are shown in **Figure 12**. The net effect of including the corrections is to decrease the nucleon attenuation length at sea level by about 7%. This correction becomes less significant with altitude [33, 52].

Cosmic ray sea-level flux datum

We showed in Figure 8 the calculations of the sea-level spectrum of particles at New York City, our flux datum site. These calculations have been compared to experimental values (see [54] for proton data, [55] for neutron data, and [56] for pion data), and they appear accurate to better than 2× for high energies, above 1 GeV. However, we are particularly concerned about the flux of lower-energy neutrons, since these are responsible for more than half of the terrestrial soft errors [57]. The limited testing to date suggests that all energetic hadrons have about the same cross section for producing soft fails (at the same particle velocity) [28]. **Figure 13** shows a collection of the available data on low-energy neutron cosmic ray flux. Of particular note are the two sets of data identified as □, which resulted from a four-year study sponsored by IBM to specifically understand the terrestrial flux of neutrons between 10 and 200 MeV. As can be seen by the data scatter in the figure, there is a scatter of 5× between various measurements, with the brilliant early work by Hess (1959) [58] running through the middle of most of the later data.

- *Absolute neutron flux*

Figure 13 shows a collection of experimental neutron spectra measurements [59]. The data points in Figure 13 are discussed below. Data which have been corrected are noted.

- *Reference [58]* These points are usually called the "Hess values." This is the most comprehensive paper on sea-level neutrons. Detectors were flown over northern latitudes at a series of altitudes. This work is so influential that its results may have contaminated later works, which always refer to Hess as the benchmark values. The high-energy values of Hess contained a mistake, which was later corrected by [52].
- *Reference [52]* The authors pointed out that the Hess detector would convert some of the other cascade particles into neutrons, erroneously increasing the measured neutron flux. This problem they called the "multiplicity" effect, and these criticisms were later verified by many other studies. We show in Figure 13 the Hess values up to 100 MeV, and above this are shown the corrected values of [58], which removes the counting of detector-generated neutrons. Since the Hess values were determined from an omnidirectional neutron detector, no correction was made for solid angle

[1] P. H. Stoker and M. Potgieter, University of Potchefstroom, Potchefstroom, South Africa (private communication).

(note that the ordinate in Figure 13 is for a total, 4πsr, flux).

■ *Reference [54]* This paper by Ashton et al. is considered very reliable. The authors come from one of the foremost cosmic ray institutes in the world, the University of Durham, U.K. Ashton's values for other cosmic ray fluxes are considered benchmarks. His analysis of the problems of measuring neutron fluxes makes this paper one of the most important in the field. (Note: The values in Figure 13 from [54] have been corrected for solid angle.)

▲ *Reference [60]* These data are from a Ph.D. thesis. For the sea-level spectrum, the author detected only 29 high-energy neutrons. Large corrections were applied to the data to obtain the final neutron flux spectrum, but no quantitative correction values were given in the paper. The paper has a figure showing good agreement between their data and Hess's data, but Hess's values are plotted erroneously about 10× lower than the actual values. It may be that the data in [60] are just plotted 10× too low, but as they stand, the results are suspect.

○ *Reference [61]* These sea-level data are an afterthought in the paper. The authors used a balloon flight to probe the neutron flux at high altitudes. Before the flight they let the detector sit in a barn at the launch site in Missouri for two weeks and collected 12 hours of data. The flux shown is the result of the pre-launch data, and is of marginal quality.

△ *Reference [62]* This is a paper from Wolfendale's group at the University of Dundee, Scotland. Wolfendale is the editor of a famous book on sea-level cosmic rays, and he has co-authored many papers on measurements of sea-level cosmic particles. This work is for the cosmic ray proton flux at sea level. The data have been corrected for solid angle.

□ *Reference [59]* This is a Ph.D. thesis (R. Saxena), sponsored at the University of New Hampshire by IBM in an attempt to use modern technology to get the best possible neutron flux spectrum for the energy range of 10–200 MeV. The results are in reasonable agreement with the previous work, although they show a slightly *harder* flux, i.e., more particles in the important energy range near 100 MeV, than seen by any previous workers. This experiment is continuing.

One major problem in using the data shown in Figure 13 is that all of the experiments except that of Hess used spectrometers with small acceptance solid angles; i.e., they measured only a small portion of the incident neutrons. Only the Durham experiments [54] made flux measurements at more than one angle and determined an accurate total flux measurement. This is a significant correction, as noted below. The angular dependence of the neutron flux spectrum enters into the neutron flux experiments in two ways (the angular dependence of the flux describes how the flux intensity varies with the angle of the flux to a sea-level plane). First, the scientist must understand the angular efficiency of the detector, and must correct the detector's measured flux for this variation in detection efficiency. Second, since most detectors do not detect neutrons from all angles, the measured flux intensity must be corrected to report a total, 4π, neutron flux.

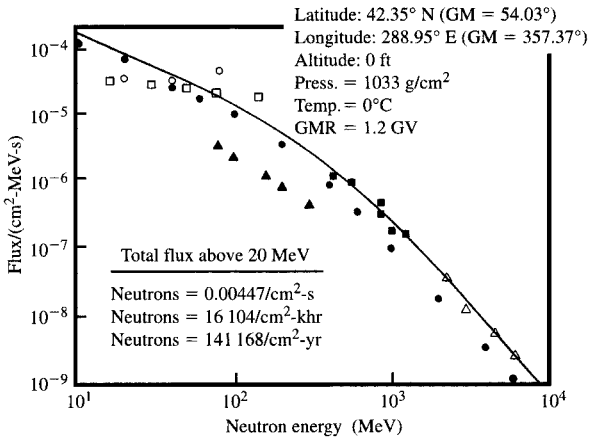

Figure 13

Experimental data on sea-level neutron spectrum. The absolute flux of neutrons above 10 MeV has been measured by six groups. These are shown on the plot and are discussed in detail in the text. All have been normalized to New York City, 1985, as a datum. The solid curve is the nominal sea-level neutron flux which best fits the data. Although the data were quoted as specific for neutrons, some of the experiments did not remove the contribution of other hadron particles. The curve is suggested as the total nucleon flux curve.

Most of the papers discussed above have assumed a cosine distribution for the incident neutron flux (the flux intensity goes as cosine θ, where $\theta = 0$ at the zenith). This is clearly wrong. The following are the experimental evaluations of the angular distribution of cosmic ray nucleons (neutron energy = E_n) at sea level: Reference [63] shows $\cos^3$ for E_n = 200 MeV; [55] shows $\cos^1$ to $\cos^4$ for $E_n > 350$ MeV; [64] shows $\cos^3$ to $\cos^5$ for E_n = 100 – 1000 MeV; [60] shows $\cos^{3.5}$ for E_n = 200 MeV; [56] shows $\cos^{2.1}$ to $\cos^{2.6}$ for E_n from 60 to 750 MeV; and [61] shows a $\cos^3$ variation for E_n from 10 to 100 MeV.

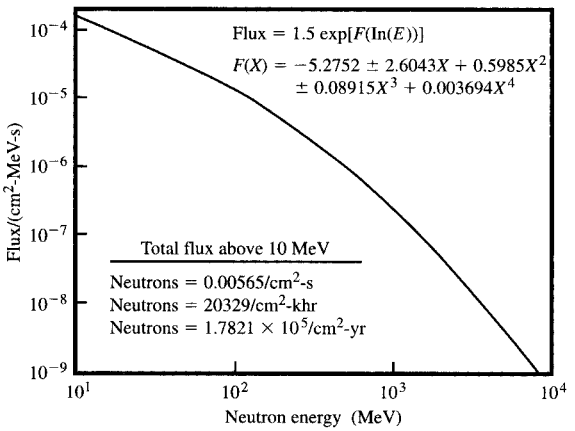

Figure 14

The proposed flux of neutrons at New York City, with the analytic formula to reproduce it to within 1%. The curve is valid from 10 MeV to 10 GeV. The integrated flux of neutrons above 10 MeV is shown in several units.

A reasonable average of the above is an angular variation of $\cos^3$ for sea-level nucleons from 20 to 1000 MeV.

The correction to a measured vertical neutron flux (in units of flux/sr) to obtain a total flux should be as follows: If the flux is presumed to be isotropic, the total flux is just 2π times the flux/sr in a vertical direction (energetic neutrons come only from above, not from below). If one assumes a cosine distribution, the multiplicative factor is just π. The general solution for a flux with an angular distribution of $\cos^x$ is the total flux = $2\pi/(x + 1)$ times the vertical flux.

Using the above experimental average of $\cos^3$ for the neutron angular flux, *the total flux is 1.6 times the vertical flux/sr*. This is referred to below as the "*solid-angle correction*."

Another problem with the experimental neutron flux papers is that there is always a correction applied for geomagnetic latitude to obtain a normalized value at 44°N (a traditional datum latitude for sea-level measurements). These papers usually used the data of [65], similar to data shown in Figure 10.

Figure 14 shows our proposed neutron flux datum, corrected to New York City (42°N, 289°E) with a simple analytic formula for the flux (the formula is valid only over the range of neutron energies shown). We have had to take the vertical flux quoted in some of the papers and make assumptions about how to estimate the total flux from the value of the directional flux (as discussed above). This nominal neutron flux value has been shown to be accurate to better than 2× [66]. We have not tried to fit the bump from 50 to 150 MeV, the □ data in Figure 13, since the authors indicated that further corrections to their data may be necessary, and the bump might disappear. Note that since this is a differential flux spectrum (neutrons/MeV), these data indicate a nonconservation of particles. There are more high-energy particles than low-energy particles in the region of the bump. This violates particle cascade theory, which indicates that there are always more lower-energy particles unless there is an absorption process which opens up with an upper-energy threshold. This is possible, as all things are possible, but the authors do not explain why it might occur.

Calculations of terrestrial geomagnetic rigidity

• *Conversion of geographic to geomagnetic coordinates*
The geomagnetic longitude and latitude of a location are based on the magnetic pole of the earth rather than the axial pole. The origin of the geomagnetic longitudes is arbitrary in the same way that in the geographic coordinate system the observatory in Greenwich, England, was once chosen as the zero point for measuring longitude. For geomagnetic longitudes, the great circle going through both the geographic and geomagnetic poles has been chosen as the zero longitude arc, with the portion going through America being zero and the portion going through the Indian Ocean being 180° (**Figure 15**).

Once the geographic coordinates of a point are specified, one must understand the rotation of coordinates in spherical geometry to go to the equivalent geomagnetic coordinates. The earth's magnetic pole currently is at 68.95 West longitude and 78.32 North latitude [17]. The magnetic pole is about 800 miles from the spin pole of the earth, at the same geographic longitude as Maine, and about 100 miles north of the Arctic Circle.

The variation of the earth's magnetic field with time is shown in **Figure 16**. This figure indicates that over 150 years the equatorial field strength has changed less than 10%. Since the terrestrial cosmic ray flux varies sublinearly with field strength, the relative cosmic ray intensities between cities should not change significantly from those tabulated in the Appendix.

The shape of the earth's magnetic field is not simply that of a dipole field (**Figure 17**). At sea level, the magnetic field intensity is made complex by the existence of two field maxima in the northern hemisphere, one in Canada and one in the U.S.S.R. The southern hemisphere has a single maximum located between Australia and Antarctica. The equatorial region is complex, with a field minimum observed near Brazil. The magnetic field

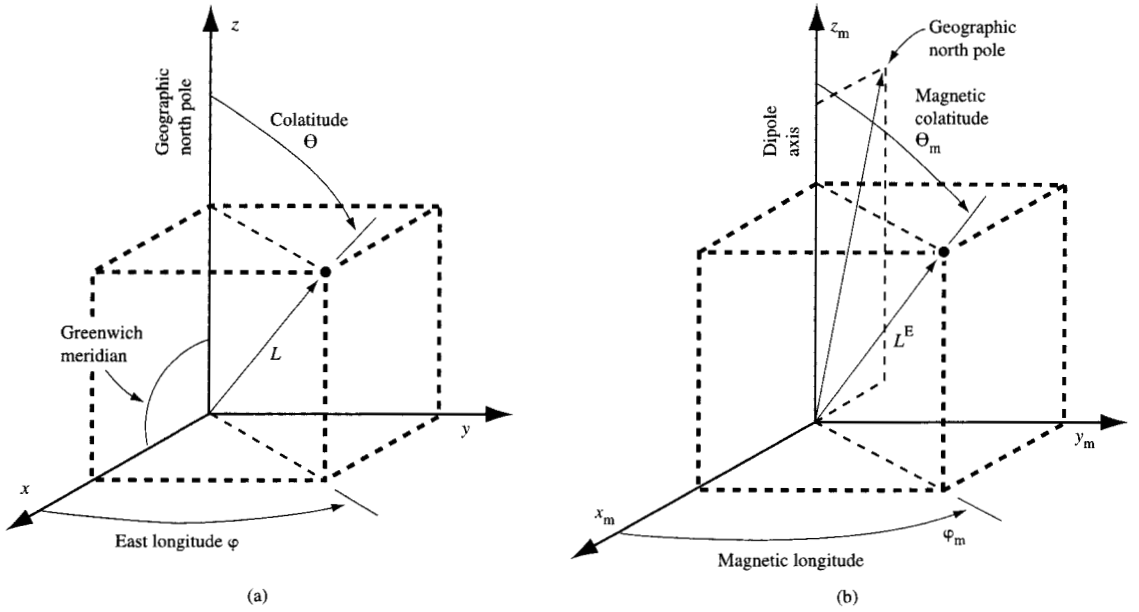

Coordinate systems for (a) geographic and (b) geomagnetic systems. The geographic longitude is zero at the Greenwich meridian, and the geographic latitude is zero at the earth's spin equator. The geomagnetic coordinate system has its poles at the magnetic poles of the earth, with the geomagnetic longitude being defined as zero at the great circle going through both the geomagnetic pole and the magnetic pole of the earth. This means that the geomagnetic coordinate system is inclined 11.5° from the geographic system if the geomagnetic north pole is fixed at 78.5° N, 291° E. From [17], reproduced with permission.

magnitudes shown in Figure 17 do not indicate regions of high or low cosmic ray intensities because the directions of the fields are not shown. Fields near the equator, which are the weakest sea-level fields, actually are very efficient in shielding cosmic ray penetration because the fields are parallel to the earth's surface. The intense fields near the magnetic poles do not shield the earth from cosmic rays because these fields are more vertical.

To convert from geographic to geomagnetic coordinates, we use the following relations (Figure 15). Define $Long_{\mathrm{MPole}}$ and Lat_{MPole} as the geographic longitude and latitude of the magnetic pole, $Long_{\mathrm{Geo}}$ and Lat_{Geo} as the geographic coordinates of a location, and $Long_{\mathrm{GM}}$ and Lat_{GM} as the final geomagnetic coordinates of the location. The spherical geometry equations we use are

$$Lat_{\mathrm{GM}} = \sin^{-1}[\cos(Lat_{\mathrm{MPole}})\cos(Lat_{\mathrm{Geo}})\cos(Long_{\mathrm{Geo}} - Long_{\mathrm{MPole}} + \sin(Lat_{\mathrm{MPole}})\sin(Lat_{\mathrm{Geo}})] \quad (6)$$

and

$$Long_{\mathrm{GM}} = \cos^{-1}\left[\frac{\tan(Lat_{\mathrm{GM}})}{\tan(X)}\right], \quad (7)$$

where

$$X = \pi - Lat_{\mathrm{MPole}} - \tan^{-1}[(\pi/2 - Lat_{\mathrm{Geo}})\cos(Long_{\mathrm{Geo}} - Long_{\mathrm{MPole}})]. \quad (8)$$

When these equations are used, it may be necessary to add or subtract units of 180° to keep within normal latitude and longitude conventions.

• *Calculation of geomagnetic rigidity*

The geomagnetic rigidity of a location was discussed above. Cosmic rays are charged particles which interact with the geomagnetic field so that their trajectory is constantly curving; see Figure 9. This magnetic bending significantly changes the flux of particles which finally reach sea level. The traditional way to evaluate this shielding effect of the magnetic field is to calculate minimum magnetic rigidities. This rigidity is the minimum energy a proton must have to penetrate to sea level at a given location (see the previous discussion on latitude effects). For a location, all possible azimuthal angles of

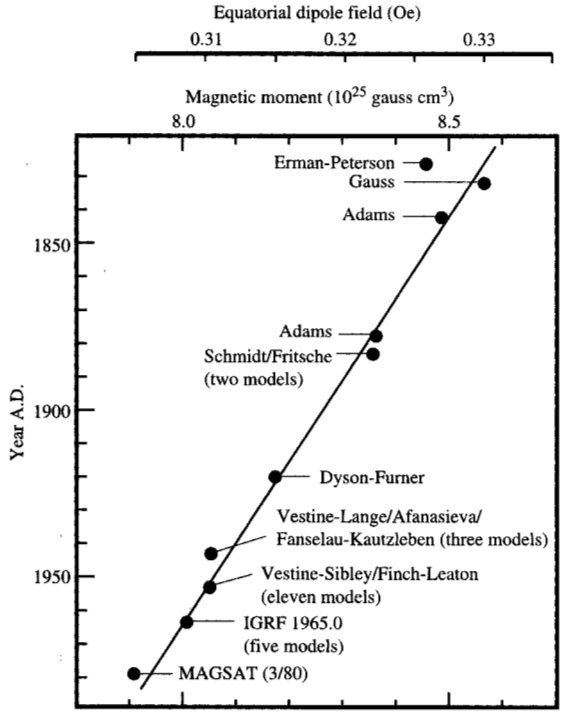

Figure 16

This plot shows the historical scientific study of Vestine on the magnetic field strength of the earth [67]. Over the entire period of recorded data, the dipole strength has been decreasing at an average rate of about 0.05% per year (16 nT per year at the equator). From [67], reproduced with permission.

incidence are considered for particles with various proton momenta until the minimum momentum for sea-level penetration is found.

Figure 18 shows a plot of geomagnetic rigidity for the earth for reference year 1980. Note that there is little resemblance between Figure 18 and Figure 17 (which shows magnetic field magnitude), since Figure 17 does not indicate field direction. The maximum geomagnetic rigidity shown in Figure 18 is located in the Indian Ocean and extends from southern India through Burma and southeast Asia to the Philippines. No cosmic ray particle with an energy below 17 GeV is presumed to penetrate to sea level in this region. Sites in this region, e.g., Yemen or India, will have a cosmic ray intensity about half that of New York City. In contrast, a location directly at the magnetic pole would have an intensity only 2% greater than that at New York City because the small rigidity of NYC, 2.64 GV, screens out only 2% of the cosmic rays. This may seem strange, for there may be 10^6 protons/m^2-s in the solar wind hitting the earth's atmosphere. However, these particles cannot just drop down into the magnetic pole, which has zero-GV magnetic rigidity, since the poles do not face the sun. The solar wind particles must enter the pole regions obliquely, and they quickly spiral away from the magnetic pole and into regions with rigidities of 1 to 2 GV.

Relative nucleon flux at major cities

In the Appendix, we present the terrestrial flux of particles at sites on earth compared to our datum flux (New York City), for which we have shown quantitative particle fluxes. We use experimental values for the change in the neutron flux with altitude, and cascade-calculation mean attenuation lengths for the other particles. We follow the recipe below:

1. Determine the geographic longitude and latitude, and the altitude of the site, plus date.
2. Use the geographic coordinates to determine the geomagnetic coordinates of the site:

$$Lat_{GM} = \sin^{-1}[\cos(Lat_{MPole})\cos(Lat_{Geo})\cos(Long_{Geo}) - Long_{MPole} + \sin(Lat_{MPole})\sin(Lat_{Geo})], \quad (6)$$

where

$$X = \pi - Lat_{MPole} - \tan^{-1}[(\pi/2 - Lat_{Geo})\cos(Long_{Geo} - Long_{MPole})]. \quad (8)$$

3. Use the most recent tables of geomagnetic coordinates vs. cutoff rigidity to calculate the site's rigidity, or use Figure 18 to interpolate to obtain the same cutoff data.
4. Convert the altitude to atmospheric density at the site using

$$A = 1033 - (0.03648H) + (4.26 \times 10^{-7}H^2). \quad (5)$$

5. Use the date to determine the position in the solar cycle using Table 1.
6. Use Figure 11 to evaluate the correct mean attenuation length for neutrons (using the geomagnetic coordinates and the site atmospheric depth). Calculate the relative neutron flux using

$$I_1 = I_2 \exp\left(\frac{A_2 - A_1}{L}\right). \quad (4)$$

7. Use the mean attenuation lengths in Table 3 for all other particles. Calculate the relative flux using Equation (4).

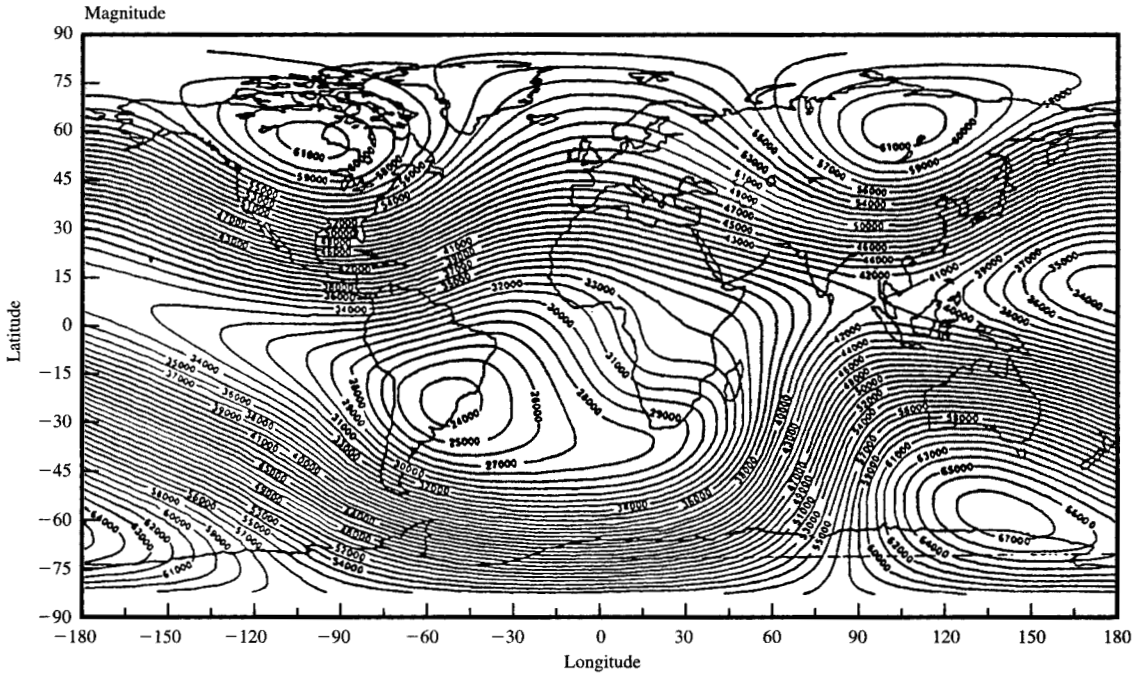

Figure 17

This plot shows the constant total field at the surface of the earth as modeled for the International Geophysical Reference Year—1980 [68]. The model which produced the above plot is based on fitting experimental evaluations of the earth's field with a theory that the field is generated by a self-exciting dynamo system in which an emf generated by the motion of a conductor (molten iron) in a magnetic field produces a current so oriented as to produce the excitation field. The dipole part of the field is assumed to result from a major two-dimensional circulation, while the non-dipole regional anomalies arise from eddy circulations in the outer layer of the core. These anomalies are fitted by assuming that within the core there are nine dipoles of various strengths which are equivalent to circulation vortices. This work is largely based on the analysis of data produced by the NASA MAGSAT satellite. From [68], reproduced with permission.

Appendix A: Cosmic ray flux at cities of the world

• *Cosmic ray flux at New York City (datum)*

To the best of our knowledge, all energetic hadrons (protons, neutrons, and pions) act similarly in producing soft fails; i.e., they are interchangeable. We have discussed their individual flux at sea level, and can combine these into a single flux in units of particles/(cm^2-MeV-s).

$$\text{Sea-level flux at datum} = 1.5 \exp [F(E)], \tag{9}$$

where

$$F(E) = -5.2752 - 2.6043 \ln E - 0.5985 (\ln E)^2 - 0.08915 (\ln E)^3 + 0.003694 (\ln E)^4,$$

where E is the particle energy in MeV. The small multiplicative correction term, 1.5, was added after extensive experimental data, covering thousands of chips, showed that this correction was necessary to correlate the flux with observed fail rates. The table which follows indicates the flux rates at cities of the world, relative to that of the flux datum above, in the following geographical locations: United States, Canada, Mexico, the Caribbean Islands, Central America, South America, Europe, Africa, Asia, and Pacific Ocean sites.

The columns are self-explanatory, with all latitudes and longitudes being given in degrees and minutes, altitudes in feet, geomagnetic values in degrees (with decimal), barometric pressure in g/cm^2, and cosmic intensity in relation to New York City. All positive longitudes are West Longitude, and negative values indicate East. All positive latitudes are North Latitude, and negative values indicate South. For reference, barometric pressure may be converted to other units by using the relationships

1033 g/cm^2 = 1013 mbar = 29.92 in. Hg = 760 mm Hg.

The last column, the *relative cosmic ray intensity* of the site, can be used to scale the soft-fail rate of a computer

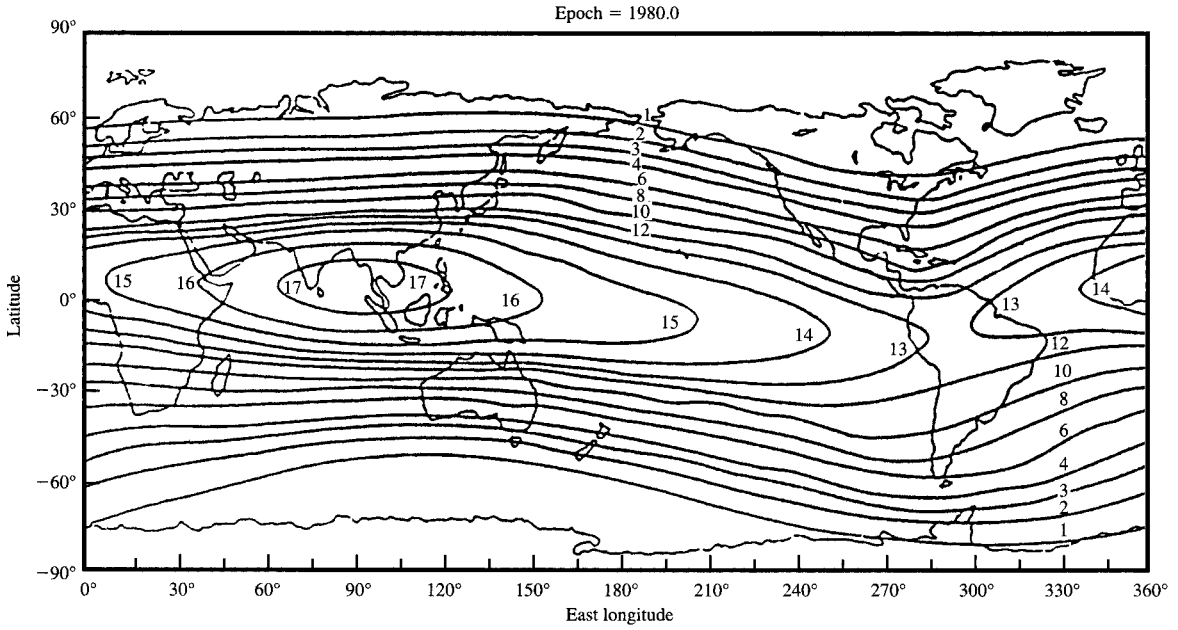

Fig. 6

Iso-rigidity contours of the vertical cosmic ray effective cutoff rigidities for Epoch 1980.0. The units of the cutoff rigidity are in GV. From [17], reproduced with permission.

system from the datum, New York City. For example, Leadville, Colorado, in the United States will have a fail rate about 13× of the datum. This number has been verified experimentally at the IBM laboratory in Leadville [57].

Relative cosmic ray intensities for cities

The table lists major cities of the world, with their geographic latitude, longitude, and altitude. These are converted to geomagnetic latitude and longitude, and to nominal barometric pressure. The geomagnetic coordinates are used to interpolate to find the magnetic rigidity of the site. This value, plus the barometric pressure, allows the calculation of the relative cosmic ray intensity. The sea-level site at New York City has been chosen as a convenient datum, and all intensities are listed relative to this flux.

For those interested in extremes, the highest cosmic ray intensities occur at

	Geographic		*Altitude* (ft)	*Geomagnetic*		*Barom. press.* (g/cm^2)	*Magn. rigid.* (GV)	*Cosmic intensity* (NYC = 1)
	Long. West	*Lat. North*		*Long. West*	*Lat. North*			
Sucre, BRAZIL	65-16	−19-1	9331	+356.0	+30.7	729	11.26	5.69
Flagstaff, Arizona, USA	111-39	35-11	6900	+49.6	+43.3	801	2.53	5.96
La Paz, BOLIVIA	68-9	−16-30	11910	+359.1	+28.2	658	12.03	8.80
Leadville, Colorado, USA	104-58	39-45	10200	+43.3	+48.8	705	1.85	12.86
The lowest cosmic ray intensities occur at								
Bombay, INDIA	−72-50	18-58	37	+218.0	+9.9	1031	16.36	0.53
Calcutta, INDIA	−88-22	22-31	21	+202.0	+11.8	1032	15.67	0.54
Bangkok, THAILAND	−100-31	13-45	26	+191.2	+2.3	1032	15.71	0.54
Rangoon, BURMA	−96-9	16-46	20	+194.6	+5.5	1032	15.59	0.55

UNITED STATES	*State*	*Geographic*		*Altitude* (ft)	*Geomagnetic*		*Barom. press.* (g/cm^2)	*Magn. rigid.* (GV)	*Cosmic intensity* (NYC = 1)
		Long. West	*Lat. North*		*Long. West*	*Lat. North*			
Albuquerque	NM	106-39	35-40	4945	+044.0	+43.9	863	2.87	3.63
Anchorage	AK	149-59	61-10	118	+102.3	+60.8	1028	0.17	1.06
Atlanta	GA	084-22	33-45	1050	+018.2	+44.9	995	4.59	1.23
Austin	TX	097-43	30-15	505	+033.0	+40.3	1014	4.28	1.08
Baltimore	MD	076-35	39-16	20	+009.4	+50.8	1032	2.44	1.01
Boston	MA	071-30	42-20	21	+002.6	+54.0	1032	2.41	1.01
Cheyenne	WY	104-48	41-50	6100	+043.5	+50.1	826	1.28	5.10
Chicago	IL	087-37	41-51	595	+023.2	+52.8	1011	1.86	1.20
Dallas	TX	096-46	32-46	435	+032.4	+42.9	1017	3.98	1.07
Denver	CO	104-58	39-45	5280	+043.3	+48.8	852	1.85	4.11
Detroit	MI	083-30	42-18	585	+017.7	+53.6	1011	2.05	1.20
Helena	MT	112-10	46-34	4155	+053.7	+54.4	888	0.74	3.16
Honolulu	HI	157-51	21-17	21	+093.4	+21.1	1032	7.23	0.82
Houston	TX	095-20	29-45	40	+030.3	+40.0	1031	4.80	0.93
Kansas City	MO	094-35	39-40	750	+031.1	+49.4	1005	2.58	1.24
Las Vegas	NV	115-70	36-10	2030	+053.7	+43.7	960	2.26	1.76
Los Angeles	CA	118-13	34-2	340	+056.5	+41.1	1020	2.46	1.11
Memphis	TN	090-30	35-80	275	+025.0	+45.9	1023	3.46	1.05
Miami	FL	080-11	25-45	10	+012.7	+37.2	1032	7.79	0.80
Milwaukee	WI	087-54	43-10	635	+023.8	+53.9	1010	1.69	1.22
Minneapolis	MN	093-15	44-59	815	+030.8	+55.4	1003	1.07	1.29
Nashville	TN	086-46	36-90	450	+021.3	+47.2	1016	3.47	1.10
New Orleans	LA	090-30	29-57	5	+024.3	+40.7	1032	4.78	0.93
New York	NY	073-58	40-45	55	+006.3	+52.4	1030	2.64	1.02
Omaha	NE	095-56	41-15	1040	+033.1	+51.4	995	1.62	1.36
Providence	RI	071-24	41-48	80	+003.1	+53.5	1030	2.42	1.03
Raleigh	NC	078-37	35-45	365	+011.6	+47.2	1019	3.88	1.06
Rochester	NY	077-35	43-90	515	+010.9	+54.7	1014	2.26	1.17
Salt Lake City	UT	111-52	40-45	4390	+051.5	+48.7	881	1.58	3.30
San Francisco	CA	122-24	37-45	65	+062.0	+44.0	1030	1.90	1.04
San Juan	PR	066-30	18-27	35	+356.8	+30.1	1031	11.19	0.68
Seattle	WA	122-20	47-35	10	+065.7	+53.6	1032	0.65	1.03
St. Louis	MO	90-11	38-36	455	+025.8	+49.3	1016	2.93	1.13
Washington	DC	077-00	38-54	25	+09.9	+50.4	1032	2.43	1.01

CANADA	*Geographic*		*Altitude* (ft)	*Geomagnetic*		*Barom. press.* (g/cm^2)	*Magn. rigid.* (GV)	*Cosmic intensity* (NYC = 1)
	Long. West	*Lat. North*		*Long. West*	*Lat. North*			
Calgary	114-50	51-20	3428	+58.1	+58.4	912	0.35	2.63
Montreal	073-35	45-30	104	+06.0	+57.1	1029	1.63	1.05
Ottawa	075-41	45-25	284	+08.7	+57.0	1022	1.40	1.11
Toronto	079-22	43-39	273	+13.2	+55.1	1023	1.49	1.10
Vancouver	123-70	49-16	38	+67.4	+55.0	1031	0.36	1.04
Burlington	079-46	43-18	281	+13.7	+54.7	1022	1.93	1.11
Winnipeg	097-90	49-53	757	+37.2	+59.8	1005	0.64	1.27

MEXICO	*Geographic*		*Altitude* (ft)	*Geomagnetic*		*Barom. press.* (g/cm^2)	*Magn. rigid.* (GV)	*Cosmic intensity* (NYC = 1)
	Long. West	*Lat. North*		*Long. West*	*Lat. North*			
Acapulco	099-54	16-50	13	+33.5	+26.7	1032	10.61	0.69
Mexico, D.F.	099-90	19-23	7546	+33.0	+29.4	781	10.18	4.24
Puebla	098-11	19-20	7094	+31.9	+29.1	795	10.42	3.77
Torreon	103-26	25-32	3708	+38.6	+35.0	903	6.54	2.20

CARIBBEAN/ATLANTIC	*Geographic*		*Altitude* (ft)	*Geomagnetic*		*Barom. press.* (g/cm^2)	*Magn. rigid.* (GV)	*Cosmic intensity* (NYC = 1)
	Long. West	*Lat. North*		*Long. West*	*Lat. North*			
Nassau, BAHAMAS	077-20	25-5	18	+009.5	+36.6	1032	7.72	0.80
Hamilton, BERMUDA	064-46	32-16	158	+355.1	+43.9	1027	6.28	0.90
Havana, CUBA	082-22	23-7	161	+015.0	+34.5	1027	9.34	0.76
Kingston, JAMAICA	076-48	18-0	110	+008.6	+29.6	1028	11.57	0.68
San Juan, PUERTO RICO	066-70	18-28	57	+356.9	+30.1	1030	11.18	0.68

CENTRAL AMERICA	*Geographic*		*Altitude* (ft)	*Geomagnetic*		*Barom. press.* (g/cm^2)	*Magn. rigid.* (GV)	*Cosmic intensity* (NYC = 1)
	Long. West	*Lat. North*		*Long. West*	*Lat. North*			
San Jose, COSTA RICA	084-50	09-56	3845	+16.0	+21.2	899	13.31	1.51
San Salvador, EL SALVADOR	089-11	13-41	2290	+21.7	+24.6	951	12.65	1.09
Guatemala City, GUATEMALA	090-31	14-37	4928	+23.2	+25.4	863	11.67	2.14
Panama City, PANAMA	079-31	08-56	118	+11.2	+20.4	1028	13.58	0.62

SOUTH AMERICA	*Geographic*		*Altitude* (ft)	*Geomagnetic*		*Barom. press.* (g/cm^2)	*Magn. rigid.* (GV)	*Cosmic intensity* (NYC = 1)
	Long. West	*Lat. North*		*Long. West*	*Lat. North*			
Buenos Aires, ARGENTINA	058-27	−34-35	82	+347.5	+46.0	1030	4.57	0.95
La Paz, BOLIVIA	068-9	−16-30	11910	+359.1	+28.2	658	12.03	8.80
Brasilia, BRAZIL	047-55	−15-47	3809	+337.3	+26.6	900	13.12	1.52
Sucre, BRAZIL	065-16	−19-1	9331	+356.0	+30.7	729	11.26	5.69
Santiago, CHILE	070-39	−33-27	1706	+2.0	+45.1	972	4.48	1.47
Bogotá, COLOMBIA	074-5	04-35	8675	+5.3	+16.2	748	14.31	4.05
Lima, PERU	077-3	−12-3	505	+8.7	+23.6	1014	13.24	0.69
Montevideo, URUGUAY	056-11	−34-53	72	+344.8	+46.2	1030	4.28	0.96
Caracas, VENEZUELA	066-54	10-30	3025	+357.8	+22.2	926	13.78	1.22

EUROPE	*Geographic*		*Altitude* (ft)	*Geomagnetic*		*Barom. press.* (g/cm^2)	*Magn. rigid.* (GV)	*Cosmic intensity* (NYC = 1)
	Long. West	*Lat. North*		*Long. West*	*Lat. North*			
Vienna, AUSTRIA	16-22	48-12	663	+294.9	+54.3	1009	2.80	1.19
Brussels, BELGIUM	4-20	50-49	328	+280.7	+54.5	1021	3.49	1.06
Copenhagen, DENMARK	12-34	55-40	16	+286.5	+60.7	1032	1.53	1.03
Helsinki, FINLAND	24-58	60-10	39	+296.9	+67.2	1031	0.74	1.04
Paris, FRANCE	2-19	48-51	197	+279.7	+52.2	1025	3.25	1.04
Strasbourg, FRANCE	7-45	48-34	932	+285.5	+53.0	999	3.67	1.24
Berlin, GERMANY	13-22	52-32	112	+289.3	+57.9	1028	1.97	1.06
Bonn, GERMANY	7-5	50-44	197	+283.7	+54.9	1025	2.96	1.05
Frankfurt, GERMANY	8-41	50-6	322	+285.7	+54.7	1021	3.40	1.07
Hamburg, GERMANY	10-0	53-32	20	+285.1	+58.2	1032	2.38	1.01
Munich, GERMANY	7-37	51-58	197	+283.5	+56.2	1025	2.23	1.07
Athens, GREECE	23-43	37-58	453	+306.8	+45.6	1016	5.15	1.03
Budapest, HUNGARY	19-5	47-30	377	+298.2	+54.1	1019	3.05	1.10
Reykjavik, ICELAND	338-43	64-9	92	+247.1	+61.8	1029	1.56	1.05
Dublin, IRELAND	354-24	53-19	51	+269.4	+54.9	1031	2.94	1.01
Milan, ITALY	9-11	45-28	397	+288.4	+50.3	1018	3.64	1.08
Naples, ITALY	14-15	40-49	33	+295.6	+46.8	1031	5.30	0.91
Rome, ITALY	12-29	41-54	66	+293.3	+47.5	1030	4.80	0.94
Amsterdam, NETHERLANDS	4-54	52-23	5	+280.4	+56.1	1032	2.59	1.01
Oslo, NORWAY	10-45	59-55	315	+281.1	+64.3	1021	1.28	1.12
Warsaw, POLAND	21-0	52-15	348	+298.0	+59.0	1020	1.94	1.12
Lisbon, PORTUGAL	351-31	38-43	312	+273.0	+40.3	1021	7.97	0.86

EUROPE (continued)	Geographic		Altitude (ft)	Geomagnetic		Barom. press. (g/cm^2)	Magn. rigid. (GV)	Cosmic intensity (NYC = 1)
	Long. West	*Lat. North*		*Long. West*	*Lat. North*			
Madrid, SPAIN	356-59	40-24	2100	+277.8	+43.0	958	7.16	1.41
Stockholm, SWEDEN	18-2	59-19	144	+289.6	+65.2	1027	0.74	1.07
Bern, SWITZERLAND	7-28	46-57	1877	+285.9	+51.4	966	3.84	1.58
Geneva, SWITZERLAND	6-9	46-12	1411	+284.9	+50.4	982	3.44	1.43
Istanbul, TURKEY	28-58	41-0	131	+311.8	+49.4	1028	4.54	0.97
Birmingham, U.K.	358-46	52-29	425	+274.2	+54.9	1017	2.94	1.12
Edinburgh, U.K.	357-28	55-57	441	+270.7	+57.9	1016	2.41	1.14
Liverpool, U.K.	357-0	53-23	198	+271.9	+55.4	1025	2.55	1.06
London, U.K.	360-35	51-30	149	+276.5	+54.4	1027	3.40	1.02
Manchester, U.K.	358-25	53-28	125	+273.2	+55.8	1028	2.35	1.05
Southampton, U.K.	359-16	50-54	65	+275.6	+53.5	1030	3.69	0.99
Gorkiy, U.S.S.R.	44-0	56-19	532	+324.2	+66.5	1013	0.60	1.19
Kiev, U.S.S.R.	30-30	50-26	440	+310.0	+58.9	1017	2.22	1.14
Leningrad, U.S.S.R.	30-15	59-55	7	+303.6	+67.9	1032	0.62	1.03
Moscow, U.S.S.R.	37-34	55-45	548	+316.0	+65.1	1013	0.82	1.19

AFRICA	Geographic		Altitude (ft)	Geomagnetic		Barom. press. (g/cm^2)	Magn. rigid. (GV)	Cosmic intensity (NYC = 1)
	Long. West	*Lat. North*		*Long. West*	*Lat. North*			
Algiers, ALGERIA	−3-2	36-46	194	+279.1	+39.6	1025	9.12	0.78
Constantine, ALGERIA	−6-37	36-21	1906	+276.8	+38.7	965	9.92	1.15
Luanda, ANGOLA	−13-14	−8-48	140	+279.6	−5.4	1027	15.72	0.56
Praia, CAPE VERDE	24.00	14-55	92	+46.7	+23.2	1029	10.41	0.71
Alexandria, EGYPT	−29-53	31-12	13	+256.3	+29.1	1032	14.96	0.56
Cairo, EGYPT	−31-15	30-2	79	+254.0	+27.4	1030	14.80	0.57
Nairobi, KENYA	−36-48	−1-17	5453	+256.3	−3.5	846	16.30	1.82
Tripoli, LIBYA	−13-11	32-54	72	+270.5	+33.8	1030	12.95	0.62
Port Louis, MAURITIUS	−57-30	2-10	181	+234.8	−4.6	1026	16.16	0.55
Casablanca, MOROCCO	17-37	33-36	164	+67.6	+38.8	1027	2.59	1.05
Lagos, NIGERIA	−3-23	6-26	9	+286.8	+10.0	1032	17.15	0.50
Capetown, SOUTH AFRICA	−18-27	33-55	40	+265.6	+33.8	1031	12.98	0.62
Johannesburg, SOUTH AFRICA	−28-2	26-10	5750	+257.7	+24.2	837	16.02	1.97
Pretoria, SOUTH AFRICA	−28-12	25-45	4375	+257.9	+23.8	881	16.04	1.46
Kinshasa, ZAIRE	−15-7	−4-17	951	+276.8	−2.4	998	16.23	0.66
Salisbury, ZIMBABWE	−31-2	17-50	4831	+256.7	+15.5	866	17.18	1.51

ASIA	Geographic		Altitude (ft)	Geomagnetic		Barom. press. (g/cm^2)	Magn. rigid. (GV)	Cosmic intensity (NYC = 1)
	Long. West	*Lat. North*		*Long. West*	*Lat. North*			
Kabul, AFGHANISTAN	−69-13	34-30	5903	+217.9	+25.5	832	14.42	2.26
Rangoon, BURMA	−96-9	16-46	20	+194.6	+5.5	1032	15.59	0.55
Phnom-Penh, CAMBODIA	−104-54	11-33	36	+196.1	−0.0	1031	15.65	0.55
Canton, CHINA	−113-15	23-7	59	+178.5	+11.4	1030	14.76	0.58
Beijing, CHINA	−116-24	39-56	171	+176.1	+28.3	1026	12.32	0.66
Shanghai, CHINA	−121-28	31-14	15	+171.4	+19.7	1032	13.89	0.59
Hong Kong, HONG KONG	−114-09	22-16	109	+177.4	+10.6	1029	14.86	0.58
Bombay, INDIA	−72-50	18-58	37	+218.0	+9.9	1031	16.36	0.53
Calcutta, INDIA	−88-22	22-31	21	+202.0	+11.8	1032	15.67	0.54
Delhi, INDIA	−77-13	28-39	770	+211.5	+18.8	1005	15.57	0.65
New Delhi, INDIA	−77-11	28-36	714	+211.5	+18.8	1007	15.57	0.64
Jakarta, INDONESIA	−106-48	−6-9	23	+186.1	−17.4	1032	12.96	0.62
Tehran, IRAN	−51-26	35-40	3908	+234.2	+29.3	896	14.30	1.46
Baghdad, IRAQ	−44-25	33-20	111	+241.2	+28.3	1028	14.95	0.58
Jerusalem, ISRAEL	−35-13	31-46	2658	+249.8	+28.4	939	14.54	1.07

ASIA (continued)	Geographic		Altitude (ft)	Geomagnetic		Barom. press. (g/cm^2)	Magn. rigid. (GV)	Cosmic intensity (NYC = 1)
	Long. West	*Lat. North*		*Long. West*	*Lat. North*			
Hiroshima, JAPAN	−132-26	34-24	95	+161.7	+23.4	1029	12.76	0.63
Osaka, JAPAN	−135-30	34-40	23	+159.0	+23.8	1032	12.28	0.64
Tokyo, JAPAN	−139-45	35-42	13	+155.8	+25.2	1032	11.86	0.65
Pyongyang, NORTH KOREA	−125-45	39-00	95	+168.5	+27.6	1029	11.36	0.68
Seoul, SOUTH KOREA	−127-01	37-33	279	+165.9	+26.3	1022	12.07	0.69
Kuwait, KUWAIT	−47-59	29-20	16	+239.8	+23.9	1032	15.53	0.55
Beirut, LEBANON	−35-30	33-53	79	+249.5	+30.5	1030	13.09	0.62
Manila, PHILIPPINES	−120-58	14-36	51	+172.4	+3.0	1031	15.32	0.56
Riyadh, SAUDI ARABIA	−46-43	24-37	1938	+241.5	+19.4	963	16.65	0.81
Singapore, SINGAPORE	−103-50	1-16	33	+189.1	−10.3	1031	14.72	0.57
Taipei, TAIWAN	−121-30	25-02	26	+171.2	+13.5	1032	14.62	0.57
Bangkok, THAILAND	−100-31	13-45	26	+191.2	+2.3	1032	15.71	0.54
Ankara, TURKEY	−32-52	39-56	2959	+250.9	+37.0	928	10.99	1.40
Ho Chi Minh City, VIETNAM	−105-50	21-01	56	+186.5	+9.4	1030	15.45	0.56

PACIFIC OCEAN	Geographic		Altitude (ft)	Geomagnetic		Barom. press. (g/cm^2)	Magn. rigid. (GV)	Cosmic intensity (NYC = 1)
	Long. West	*Lat. North*		*Long. West*	*Lat. North*			
Canberra, AUSTRALIA	−149-10	35-19	1906	+146.3	+25.8	965	11.18	1.07
Melbourne, AUSTRALIA	−145-0	37-49	114	+150.1	+27.9	1028	11.21	0.69
Sydney, AUSTRALIA	−151-11	33-53	138	+144.3	+24.6	1027	11.48	0.68
Suva, FIJI	−178-25	18-7	30	+116.4	+13.2	1031	12.80	0.62
Wellington, NEW ZEALAND	−174-51	41-28	415	+125.8	+35.3	1017	5.46	1.00
Port Moresby, NEW GUINEA	−147-7	−9-29	92	+142.5	−17.9	1029	13.73	0.61

References and notes

1. V. F. Hess, *Phys. Zeits.* **12,** 998 (1911).
2. V. F. Hess, *Phys. Zeits.* **13,** 1084 (1912).
3. G. Pfotzer, *Z. Phys.* **102,** 23 (1936).
4. See dedicated issue of the *IBM Journal of Research and Development*, Vol. 40, No. 1, January 1996, discussing how cosmic rays affect terrestrial electronic systems.
5. A. W. Wolfendale, *Cosmic Rays at Sea Level*, The Institute of Physics, London, 1973.
6. M. Garcia-Munoz, G. M. Mason, and J. A. Simpson, *Proceedings of the 12th International Conference on Cosmic Rays*, University of Tasmania, Hobart, 1971, p. 209.
7. See M. A. Shea, D. F. Smart, and K. G. McCracken, *J. Geophys. Res.* **70,** 1098 (1965); M. A. Shea and D. F. Smart, *Space Research VI*, Spartan Books, Washington, DC, 1966, p. 177; M. A. Shea and D. F. Smart, *J. Geophys. Res.* **72,** 2021 (1967); M. A. Shea, D. F. Smart, and J. R. McCall, *Can. J. Phys.* **46,** S1098 (1968); M. A. Shea, *J. Geophys. Rev.* **74,** 2407 (1969). The following papers available from the Air Force Cambridge Research Center, Hanscomb Air Force Base, Hanscomb, MA: M. A. Shea, D. F. Smart, and J. R. McCall, *Environmental Research Papers ERP-493, AFCRL-TR-0550* (1974) and *ERP-497, AFCRL-TR-0008* (1974); M. A. Shea and D. F. Smart, *Environmental Research Papers ERP-498, AFCRL-TR-0042* (1975) and *ERP-502, AFCRL-TR-0177* (1975); M. A. Shea and D. F. Smart, *Environmental Research Paper ERP-802, AFCRL-TR-82-0320* (1982).
8. M. A. Shea, D. F. Smart, and K. G. McCracken, *J. Geophys. Res.* **70,** 4117 (1965).
9. M. A. Shea, D. F. Smart, and K. G. McCracken, *J. Geophys. Res.* **70,** 1098 (1965).
10. D. F. Smart and J. R. McCall, *Environmental Research Papers ERP-493, AFCRL-TR-0550* (1974) and *ERP-497, AFCRL-TR-0008* (1974).
11. M. A. Shea and D. F. Smart, *J. Geophys. Res.* **72,** 2021 (1967).
12. M. A. Shea, D. F. Smart, and J. R. McCall, *Can. J. Phys.* **46,** 1098 (1968).
13. M. A. Shea, *J. Geophys. Rev.* **74,** 2407 (1969).
14. M. A. Shea, D. F. Smart, and J. R. McCall, *Environmental Research Papers ERP-493, AFCRL-TR-0550* (1974) and *ERP-497, AFCRL-TR-0008* (1974).
15. M. A. Shea and D. F. Smart, *Environmental Research Papers ERP-498, AFCRL-TR-0042* (1975) and *ERP-502, AFCRL-TR-0177* (1975).
16. M. A. Shea and D. F. Smart, *Environmental Research Paper ERP-802, AFCRL-TR-82-0320* (1982).
17. *Handbook of Geophysics and the Space Environment*, A. S. Jursa, Ed., Air Force Geophysics Laboratory, Air Force Systems Command, Hanscomb, MA, 1985; see chapter 4-6. Publication is available as Document No. ADA-167000 from the U.S. National Technical Information Service, Springfield, VA.
18. J. G. Wilson, *Cosmic Rays*, Springer-Verlag, New York, 1976.
19. J. A. Simpson, *Phys. Rev.* **83,** 1175 (1951).
20. J. A. Simpson, W. Fonger, and S. B. Treiman, *Phys. Rev.* **90,** 934 (1953).
21. J. A. Simpson and W. C. Fagot, *Phys. Rev.* **90,** 1068 (1953).
22. S. E. Forbush, *J. Geophys. Res.* **59,** 525 (1954).
23. K. O'Brien, H. A. Sandmeier, G. E. Hansen, and J. E. Campbell, *J. Geophys. Res.* **83,** 114 (1978).
24. K. O'Brien, *J. Geophys. Res.* **75,** 4357 (1970).
25. K. O'Brien, "The Natural Radiation Environment,"

D.O.E. Report No. 720805-P1, U.S. Department of Energy, Washington, DC, 1971, p. 15.
26. K. O'Brien, *D.O.E. Report No. EML-338*, U.S. Department of Energy, Washington, DC, 1978.
27. J. F. Ziegler, J. P. Biersack, and U. Littmark, *The Stopping and Range of Ions in Matter*, Pergamon Press, New York, 1985.
28. J. F. Dicello, M. E. Schillaci, C. W. McCabe, J. D. Doss, M. Paciotti, P. Berardo, and J. F. Dicello III, *IEEE Trans. Nucl. Sci.* **NS-32,** 4201 (1985).
29. G. Lemaitre and M. S. Vallarta, *Phys. Rev.* **43,** 87 (1933).
30. C. Stormer, *Z. Astrophys.* **1,** 237 (1930).
31. J. H. Adams, Jr., R. Silverberg, and C. H. Tsao, "Cosmic Ray Effects on Microelectronics, Part I: The Near-Earth Particle Environment," *Memorandum Report No. 4506*, Naval Research Laboratories, Washington, DC, 1981.
32. A. M. Hillas, *Cosmic Rays*, Pergamon Press, Oxford, UK, 1972.
33. H. Carmichael, M. Bercovitch, M. A. Shea, M. Magidin, and R. W. Peterson, *Can. J. Phys.* **46,** S10006 (1968).
34. J. F. Steljes, H. Carmichael, and K. G. McCracken, *J. Geophys. Res.* **66,** 1363 (1961).
35. H. Carmichael, M. Bercovitch, J. F. Steljes, and M. Magidin, *Proceedings of the International Conference on Cosmic Rays*, 1968, p. 553.
36. J. Lockwood and W. R. Weber, *J. Geophys. Res.* **72,** 3395 (1967).
37. M. V. K. Apparao, R. R. Daniel, G. Joseph, G. S. Gokale, P. J. Lavakare, and R. Sunderrajan, *Can. J. Phys.* **46,** S1030 (1968).
38. G. G. Boella, A. Degli, C. Dilworth, G. Giannelli, E. Rocca, L. Scarsi, and D. Shapiro, *Nuovo Cim.* **29,** 103 (1963).
39. J. C. Barton and M. Slade, *Proceedings of the International Conference on Cosmic Rays*, 1965, p. 1006.
40. F. Bachelet, P. Balata, E. Dyring, and N. Iucci, *Nuovo Cim.* **35,** 23 (1965).
41. D. A. Bryant, T. L. Cline, U. D. Desai, and F. B. McDonald, *J. Geophys. Res.* **141,** 478 (1965).
42. G. G. Boella, G. D. Antoni, C. Dilworth, M. Panelli, and L. Scarsi, *Earth & Planet Sci. Lett.* **4,** 393 (1968).
43. S. Fukui, *Prog. Theor. Phys. Suppl.* **16,** 1 (1060).
44. D. C. Rose, K. B. Fenton, J. Katzman, and J. A. Simpson, *Can. J. Phys.* **34,** 968 (1956).
45. B. B. Rossi, *High Energy Physics*, Prentice-Hall, Inc., Englewood Cliffs, NJ, 1954, p. 488.
46. J. Linsey, *Phys. Rev. Lett.* **10,** 146 (1963).
47. H. W. Patterson, W. N. Hess, B. J. Moyer, and R. W. Wallace, *Publication No. 8208*, University of California at Livermore, 1959.
48. H. V. Neher, *J. Geophys. Res.* **72,** 1527 (1967).
49. G. Clark, *Nuovo Cim. Suppl.* **8,** 623 (1958).
50. J. Delvaille, F. Kendziorski, and K. Greisen, *J. Phys. Soc. Jpn.* **17,** Suppl. A-III, 76 (1962).
51. M. Yamashita, L. D. Stephens, and H. W. Patterson, *J. Geophys. Res.* **71,** 3817 (1966).
52. E. B. Hughes and P. L. Marsden, *J. Geophys. Rev.* **21,** 1435 (1966).
53. B. C. Raubenheimer and P. H. Stoker, *J. Geophys. Res.* **79,** 5069 (1974).
54. F. Ashton, H. J. Edwards, and G. N. Kelly, *J. Phys. A: Gen. Phys.* **4,** 352 (1971).
55. E. Lohrmann, *Nuovo Cim.* **1,** 1126 (1955).
56. M. Conversi and P. Rothwell, *Nuovo Cim.* **12,** 101 (1954).
57. J. F. Ziegler, H. W. Curtis, H. P. Muhlfeld, C. J. Montrose, B. Chin, M. Nicewicz, C. A. Russell, W. Y. Wang, L. B. Freeman, P. Hosier, L. E. LaFave, J. L. Walsh, J. M. Orro, G. J. Unger, J. M. Ross, T. J. O'Gorman, B. Messina, T. D. Sullivan, A. J. Sykes, H. Yourke, T. A. Enger, V. Tolat, T. S. Scott, A. H. Taber, R. J. Sussman, W. A. Klein, and C. W. Wahaus, "IBM Experiments in Soft Fails in Computer Electronics (1978–1994)," *IBM J. Res. Develop.* **40,** 3 (January 1996).
58. W. N. Hess, H. W. Patterson, R. Wallace, and E. L. Chupp, *Phys. Rev.* **116,** 445 (1959).
59. J. M. Ryan and R. Saxena, "Ground Level Neutron Measurements from 10–170 MeV," *Proceedings of the 1996 Topical Meeting*, Radiation Protection and Shielding Division, American Nuclear Society, 1996, pp. 219–226; R. Saxena, Ph.D. Thesis, University of New Hampshire, Durham (unpublished).
60. E. Heidbreder, K. Pinkau, C. Reppin, and V. Schonfelder, *J. Geophys. Rev.* **76,** 2905 (1971).
61. A. M. Preszler, G. M. Simnett, and R. S. White, *J. Geophys. Rev.* **79,** 17 (1974).
62. G. Brooke and A. W. Wolfendale, *Proc. Phys. Soc.* **83,** 843 (1964).
63. N. C. Barford and G. Davis, *Proc. Roy. Soc. Lond.* **214,** 225 (1952).
64. S. Miyake, K. Hinotani, J. Katsumata, and T. Kaneco, *J. Phys. Soc. Jpn.* **12,** 845 (1957); *ibid.*, p. 113.
65. M. Conversi, *Phys. Rev.* **79,** 750 (1950).
66. T. J. O'Gorman, J. M. Ross, A. H. Taber, J. F. Ziegler, H. P. Muhlfeld, C. J. Montrose, H. W. Curtis, and J. L. Walsh, "Field Testing for Cosmic Ray Soft Errors in Semiconductor Memories," *IBM J. Res. Develop.* **40,** 41 (January 1996).
67. E. H. Vestine, *Benedum Earth Magnetism*, University of Pittsburgh Press, Pittsburgh, 1962.
68. R. A. Langel, *NASA Tech. Memo. 80698*, NASA Goddard Research Center, Greenbelt, MD, 1962.

Received February 15, 1997; accepted for publication December 5, 1997

James F. Ziegler *IBM Research Division, Thomas J. Watson Research Center, P.O. Box 218, Yorktown Heights, New York 10598 (ZIEGLER at YKTVMV, ziegler@watson.ibm.com).*
After receiving B.S., M.S., and Ph.D. degrees from Yale, Dr. Ziegler joined IBM in 1967 at the Thomas J. Watson Research Center, where he now manages the Material Analysis and Radiation Effects group. Most of his research concerns the interaction of radiation with matter. Dr. Ziegler is the author of more than 130 publications and 14 books; he holds 11 U.S. patents. He received IBM Corporate Awards in 1981 and 1990. Dr. Ziegler is a Fellow of the American Physical Society and of the IEEE. He has been awarded the von Humboldt Senior Scientist Prize by the German government.

[[Page 140 is blank]]